

# HCO<sub>3</sub><sup>−</sup> Secretion by Murine Nasal Submucosal Gland Serous Acinar Cells during Ca<sup>2+</sup>-stimulated Fluid Secretion

Robert J. Lee,<sup>1</sup> Janice M. Harlow,<sup>1</sup> Maria P. Limberis,<sup>3</sup> James M. Wilson,<sup>3</sup> and J. Kevin Foskett<sup>1,2</sup>

<sup>1</sup>Department of Physiology, <sup>2</sup>Department of Cell and Developmental Biology, and <sup>3</sup>Department of Pathology and Laboratory Medicine, Division of Medical Genetics, University of Pennsylvania, Philadelphia, PA 19104

Airway submucosal glands contribute to airway surface liquid (ASL) composition and volume, both important for lung mucociliary clearance. Serous acini generate most of the fluid secreted by glands, but the molecular mechanisms remain poorly characterized. We previously described cholinergic-regulated fluid secretion driven by Ca<sup>2+</sup>-activated Cl<sup>−</sup> secretion in primary murine serous acinar cells revealed by simultaneous differential interference contrast (DIC) and fluorescence microscopy. Here, we evaluated whether Ca<sup>2+</sup>-activated Cl<sup>−</sup> secretion was accompanied by secretion of HCO<sub>3</sub><sup>−</sup>, possibly a critical ASL component, by simultaneous measurements of intracellular pH (pH<sub>i</sub>) and cell volume. Resting pH<sub>i</sub> was 7.17 ± 0.01 in physiological medium (5% CO<sub>2</sub>–25 mM HCO<sub>3</sub><sup>−</sup>). During carbachol (CCh) stimulation, pH<sub>i</sub> fell transiently by 0.08 ± 0.01 U concomitantly with a fall in Cl<sup>−</sup> content revealed by cell shrinkage, reflecting Cl<sup>−</sup> secretion. A subsequent alkalinization elevated pH<sub>i</sub> to above resting levels until agonist removal, whereupon it returned to prestimulation values. In nominally CO<sub>2</sub>–HCO<sub>3</sub><sup>−</sup>-free media, the CCh-induced acidification was reduced, whereas the alkalinization remained intact. Elimination of driving forces for conductive HCO<sub>3</sub><sup>−</sup> efflux by ion substitution or exposure to the Cl<sup>−</sup> channel inhibitor niflumic acid (100 μM) strongly inhibited agonist-induced acidification by >80% and >70%, respectively. The Na<sup>+</sup>/H<sup>+</sup> exchanger (NHE) inhibitor dimethylamiloride (DMA) increased the magnitude (greater than twofold) and duration of the CCh-induced acidification. Gene expression profiling suggested that serous cells express NHE isoforms 1–4 and 6–9, but pharmacological sensitivities demonstrated that alkalinization observed during both CCh stimulation and pH<sub>i</sub> recovery from agonist-induced acidification was primarily due to NHE1, localized to the basolateral membrane. These results suggest that serous acinar cells secrete HCO<sub>3</sub><sup>−</sup> during Ca<sup>2+</sup>-evoked fluid secretion by a mechanism that involves the apical membrane secretory Cl<sup>−</sup> channel, with HCO<sub>3</sub><sup>−</sup> secretion sustained by activation of NHE1 in the basolateral membrane. In addition, other Na<sup>+</sup>-dependent pH<sub>i</sub> regulatory mechanisms exist, as evidenced by stronger inhibition of alkalinization in Na<sup>+</sup>-free media.

## INTRODUCTION

The secretion of airway surface liquid (ASL) and the control of its volume and composition are critical for the maintenance of mucociliary clearance and the ability to rid the lung of inspired pathogens and irritants (for review see Wine and Joo, 2004). In cartilaginous airways, submucosal exocrine glands secrete a large percentage of the NaCl-rich fluid and mucus that comprise the ASL (for review see Ballard and Inglis, 2004; Ballard and Spadafora, 2007), and a knowledge of both the regulation and composition of submucosal gland secretion is essential for understanding lung fluid homeostasis. Previous experimental studies of intact tissue preparations have provided insights into secretagogue-mediated regulation of these glands, including the rates of secretion and the volumes of the end-product secretions (Yang et al., 1988; Inglis et al., 1997a,b, 1998; Jayaraman et al., 2001; Joo et al., 2001a,b, 2002a,b, 2006; Song and Verkman, 2001; Salinas et al., 2005; Song et al., 2006; Wu et al., 2006; Ianowski et al., 2007). However, the complex structure and relative inaccessibility of airway

submucosal glands have limited experimental studies of the ionic composition of the primary secretions and the molecular mechanisms by which the various cell types (serous, mucous, and both ciliated and nonciliated collecting duct cells) secrete and/or modify the fluid/mucous product.

Of particular interest are serous acinar cells present at the distal ends of submucosal glands, because they likely secrete the bulk of glandular fluid in response to secretagogues that use cAMP and/or Ca<sup>2+</sup> as second messengers (Wu et al., 2006). The fluid secreted by serous acinar cells contributes directly to ASL volume and is also likely

Abbreviations used in this paper: AE, Cl<sup>−</sup>/HCO<sub>3</sub><sup>−</sup> (anion) exchanger; AM, acetoxymethyl; ASL, airway surface liquid; BCECF, 2',7'-bis-(2-carboxyethyl)-5-(and-6)-carboxyfluorescein; CCh, carbachol; CF, cystic fibrosis; CFTR, cystic fibrosis transmembrane conductance regulator; DAPI, 4',6-diamidino-2-phenylindole; DIC, differential interference contrast; DMA, 5-(N,N-dimethyl)amiloride; DPBS, Dulbecco's PBS; EIPA, 5-(N-ethyl-N-isopropyl)amiloride; NBC, Na<sup>+</sup>-HCO<sub>3</sub><sup>−</sup> cotransporter; NFA, niflumic acid; NHE, Na<sup>+</sup>/H<sup>+</sup> exchanger; NKCC1, Na<sup>+</sup> K<sup>+</sup> 2Cl<sup>−</sup> cotransporter isoform 1; pH<sub>i</sub>, intracellular pH; SNARE, seminaphtharhodafleur-5F 5-(and-6)-carboxylic acid; Wt, wild-type.

Correspondence to J. Kevin Foskett: foskett@mail.med.upenn.edu

crucial for proper hydration of mucin granules released from more proximal mucous cells (for review see Ballard and Inglis, 2004). Serous cells also play an important role in innate airway immunity by secreting lysozyme, lactoferrin (Raphael et al., 1989), various antimicrobial peptides such as defensins, and mucin macromolecules such as Muc7 (for reviews see Ballard and Inglis, 2004; Wine and Joo, 2004). Submucosal gland serous cells have been hypothesized to play a particularly critical role in the pathology of the disease cystic fibrosis (CF). CF is a disease caused by mutations in the cystic fibrosis transmembrane conductance regulator (CFTR), an apical membrane anion channel expressed in various epithelia, including the airway. In addition to conducting  $\text{Cl}^-$  and  $\text{HCO}_3^-$  (Poulsen et al., 1994), CFTR also may directly or indirectly regulate the activities of other ion channels and transporters, including the epithelial  $\text{Na}^+$  channel (for review see Huang et al., 2004) and  $\text{Cl}^-/\text{HCO}_3^-$  exchangers (Lee et al., 1999a,b; Park et al., 2002; Ko et al., 2004). Immunohistochemical localization studies suggest that serous acinar cells are major sites of CFTR expression in the lung (Engelhardt et al., 1992; Jacquot et al., 1993). It has therefore been hypothesized that defects in the volume and/or composition of submucosal gland secretions caused by lack of CFTR contribute to the ASL dehydration that leads to impaired mucociliary clearance and the ultimately fatal lung damage from the resultant chronic bacterial infection that is a hallmark of CF pathology.

Because of the critical role of serous acinar cells in airway fluid physiology, we previously examined the ion transport mechanisms that underlie  $\text{Ca}^{2+}$  agonist-evoked fluid secretion in primary serous cells isolated from mouse nasal turbinate and septum (Lee et al., 2007). Agonists such as acetylcholine that elevate intracellular  $[\text{Ca}^{2+}]_i$  are believed to be the major submucosal gland secretagogues in terms of the magnitude and rate of the fluid secretion response (Yang et al., 1988; Inglis et al., 1997b; Trout et al., 1998a; Joo et al., 2001b, 2002a,b; Wu et al., 2006). We combined differential interference contrast (DIC) microscopy with simultaneous quantitative fluorescence imaging of indicator dyes to measure the concentrations of ions involved in driving fluid secretion ( $\text{Cl}^-$ ) and regulating it ( $\text{Ca}^{2+}$ ). Cholinergic agonist-induced fluid secretion was shown to be reflected in cell volume changes that were indicative of changes in cell solute content underlying fluid secretion, suggesting that murine serous acinar cells secrete  $\text{Cl}^-$  and fluid in response to a rise in  $[\text{Ca}^{2+}]_i$ . The observed  $\text{Ca}^{2+}$ -evoked  $\text{Cl}^-$  secretion occurs through a  $\text{Cl}^-$  efflux pathway that is independent of CFTR, in agreement with observations of intact gland preparations from CF human lungs and CFTR-knockout (*cfr<sup>tm1Unc</sup>/-*) mice that suggested that cholinergic-stimulated fluid secretion remains intact in the absence of CFTR function (Jayaraman et al., 2001; Joo et al., 2002a; Thiagarajah

et al., 2004; Salinas et al., 2005; Song et al., 2006; Ianowski et al., 2007).

In addition to their role in  $\text{Cl}^-$  secretion, we hypothesized that airway submucosal gland serous cells are likely important for secretion of  $\text{HCO}_3^-$  into the airway. Other exocrine gland acinar cells stimulated with cholinergic agonists exhibit marked decreases in intracellular pH ( $\text{pH}_i$ ) that have been proposed to reflect loss of cellular  $\text{HCO}_3^-$  indicative of  $\text{HCO}_3^-$  secretion (Robertson and Foskett, 1994; Evans et al., 1999; Nguyen et al., 2000; Brown et al., 2003; Nguyen et al., 2004). To determine whether  $\text{Ca}^{2+}$ -mobilizing agonists stimulate  $\text{HCO}_3^-$  secretion from airway gland serous acinar cells, the DIC fluorescence microscopy technique was modified to simultaneously monitor agonist-induced cell volume changes (reflecting  $\text{Cl}^-$  secretion) and the fluorescence of seminaphtharhodafluor-5F 5-(and-6)-carboxylic acid (SNARF-5F), a quantitative ratiometric indicator of  $\text{pH}_i$  (reflecting changes in  $[\text{HCO}_3^-]_i$ ), in combination with appropriate ion substitutions and pharmacology. The results outlined below suggest that cholinergic/ $\text{Ca}^{2+}$  stimulation of serous acinar cells leads to cytoplasmic acidification that results from a net efflux of cellular  $\text{HCO}_3^-$  via a niflumic acid (NFA)-sensitive pathway shared with  $\text{Cl}^-$ . Carbachol (CCh)-induced acidification is compensated for by up-regulation of the activity of the  $\text{Na}^+/\text{H}^+$  exchanger isoform 1 (NHE1), which drives  $\text{HCO}_3^-$  secretion by raising  $\text{pH}_i$  and promoting conversion of intracellular  $\text{CO}_2$  to  $\text{HCO}_3^-$ . These data contribute to the understanding of submucosal gland fluid secretion, the composition of serous cell secretions,  $\text{HCO}_3^-$  secretion mechanisms in the airway, and the mechanisms of  $\text{pH}_i$  regulation in serous cells.

## MATERIALS AND METHODS

### Reagents

Molecular biology reagents were obtained from Invitrogen. A rabbit polyclonal antibody against the 22-amino acid C terminus of rat NHE1 (100% homologous to the mouse NHE1 C terminus) and control antigenic blocking peptide were purchased from Alpha Diagnostic International. Polyclonal antiserum against the  $\text{Na}^+ \text{K}^+ 2\text{Cl}^-$  cotransporter isoform 1 (NKCC1) was a gift from R. James Turner (National Institute of Dental and Craniofacial Research, Bethesda, MD). Anti-CFTR monoclonal antibody 24-1 was purchased from R&D Systems, Inc. All microscope filters were obtained from Chroma Technologies, Inc. Cariporide (HOE 642; (4-isopropyl-3-methylsulfonyl-benzoyl)-guanidine methanesulfonate) and S3226 (3-[2-(3-guanidino-2-methyl-3-oxo-propenyl)-5-methyl-phenyl]-N-isopropylidene-2-methyl-acrylamide dihydrochloride) were gifts from Sanofi-Aventis Deutschland GmbH. All other reagents were purchased from Sigma-Aldrich unless otherwise noted.

### Experimental Solutions

All experimental solutions were made fresh daily, with compositions listed in Table I. A vapor pressure osmometer was used to ensure that the osmolality was  $\sim 300 \text{ mOsm kg}^{-1}$ . Unless noted, experiments were performed in one of two physiological salt solutions, Solution A ( $\text{CO}_2$ - $\text{HCO}_3^-$ -buffered; gassed with 95%  $\text{O}_2$ -5%  $\text{CO}_2$ )

TABLE I  
Experimental Solution Compositions

Solution	A	B	C	D	E	F	G
NaCl	125 <sup>a</sup>	125				5	41
NMDG-Cl			125	125	120–140		
KCl	5	5	5	5	5	60	57
K-Gluconate						80	32
MgCl <sub>2</sub>	1.2	1.2	1.2	1.2	1.2		1.2
MgSO <sub>4</sub>						0.8	
CaCl <sub>2</sub>	1.2	1.2	1.2	1.2	1.2		1
Ca-Gluconate						1.6	
NaH <sub>2</sub> PO <sub>4</sub>	1.2	1.2					1.2
KH <sub>2</sub> PO <sub>4</sub>			1.2	1.2	1.2		
Glucose	11	11	11	11	11		11
Sucrose		10		10			
HEPES		10		10	10	20	
NaHCO <sub>3</sub>	25						25
NMDG-HCO <sub>3</sub>			25				
NH <sub>4</sub> Cl					0, 5, 10, or 20		
pH <sub>o</sub>	7.4	7.4	7.4	7.4	7.4	6.8, 7.2, or 7.6	7.4
gassed w/	5% CO <sub>2</sub> /95% O <sub>2</sub>	100% O <sub>2</sub>	5% CO <sub>2</sub> /95% O <sub>2</sub>	100% O <sub>2</sub>	100% O <sub>2</sub>	100% O <sub>2</sub>	5% CO <sub>2</sub> /95% O <sub>2</sub>

<sup>a</sup>All values for dissolved solids are mM.

or Solution B (HEPES-buffered, nominally CO<sub>2</sub>–HCO<sub>3</sub><sup>–</sup>-free; gassed with 100% O<sub>2</sub>). Experiments performed under Na<sup>+</sup>-free conditions (with Na<sup>+</sup> isosmotically replaced by NMDG<sup>+</sup>) were performed in Solution C. Experiments performed under both Na<sup>+</sup>- and HCO<sub>3</sub><sup>–</sup>-free conditions were performed in Solution D. Intracellular pH<sub>i</sub> buffering capacity was measured using Solution E (containing no Na<sup>+</sup> or HCO<sub>3</sub><sup>–</sup> to neutralize all mechanisms of cellular pH<sub>i</sub> regulation) with [NH<sub>3</sub>]<sub>o</sub> = 0.6, 1.2, or 2.5 mM (at pH 7.4; made via isosmotic replacement of NMDG-Cl with 5, 10, or 20 mM NH<sub>4</sub>Cl, respectively). Intracellular in vivo SNARF calibration was performed using high [K<sup>+</sup>]<sub>o</sub>. Solution F containing 10 µg/ml nigericin and pH<sub>o</sub> values of 6.8, 7.2, and 7.6. Solution G (high [K<sup>+</sup>]<sub>o</sub>, low [Cl<sup>–</sup>]<sub>o</sub>) was used to experimentally block HCO<sub>3</sub><sup>–</sup> efflux, as described in the text. In all experiments involving agonist stimulation, 100 µM CCh was used, previously shown to be a saturating concentration for both serous cells (Lee et al., 2007) and intact murine submucosal glands (Janowski et al., 2007).

Under conditions of CO<sub>2</sub>–HCO<sub>3</sub><sup>–</sup> buffering, the pH<sub>o</sub> and dissolved [CO<sub>2</sub>]<sub>o</sub> of the extracellular medium are critical, because calculation of CO<sub>2</sub>–HCO<sub>3</sub><sup>–</sup>-dependent intracellular buffering capacity (β<sub>HCO<sub>3</sub></sub>) strongly depends on [CO<sub>2</sub>]<sub>o</sub> (as described below), and because H<sup>+</sup> and HCO<sub>3</sub><sup>–</sup> transport mechanisms are likely highly sensitive to [H<sup>+</sup>] and [HCO<sub>3</sub><sup>–</sup>] gradients. Because of the high CO<sub>2</sub> permeability of plastics, the CO<sub>2</sub>–HCO<sub>3</sub><sup>–</sup>-buffered solutions were gassed in glass water-heated reservoirs connected with glass tubing to glass water-heated coils, where the solution was warmed before perfusion into the chamber containing the cells. Because a loss of dissolved [CO<sub>2</sub>]<sub>o</sub> would be reflected in a rise in pH<sub>o</sub>, solutions of 2',7'-bis-(2-carboxyethyl)-5-(and-6)-carboxyfluorescein (BCECF) free acid were used to confirm that pH<sub>o</sub> = ~7.4 for gassed Solution A in the perfusion system (as shown in Fig. 1, A and B, and described in the legend). The temperature of the perfusate inside the perfusion chamber was measured daily using a digital thermometer (VWR Scientific) and probe (YSI, Inc.) and adjusted to ~37°C.

#### Murine Nasal Serous Acinar Cell Isolation

Murine serous acinar cells were isolated as previously described (Lee et al., 2007) from adult wild-type (Wt) or *cftr*<sup>tm1Unc-/-</sup> mice

on a C57BL/6 background housed in a pathogen-free facility. Ages of the mice ranged from 3 to 7 mo. All procedures involving animals were handled according to regulations set out by the Institutional Animal Care and Use Committee of the University of Pennsylvania. In brief, nasal turbinate and septum were removed from mice killed via CO<sub>2</sub> asphyxiation followed by cervical dislocation. Tissue was immediately placed in ice-cold Solution B, minced finely with scissors, and then digested for ~45 min at room temp in CaCl<sub>2</sub>-free Solution B supplemented with 1× MEM vitamins, 1× MEM amino acids, 2 mM L-glutamine, 1.5 mg ml<sup>–1</sup> type IV collagenase (Worthington Biochemical Corp.), 0.28 U ml<sup>–1</sup> liberase enzyme blend 3 (Roche Diagnostics Corp.), 10 µg/ml DNase I, and 0.8% BSA with gentle shaking and continuous gassing of 100% O<sub>2</sub>. Cells were then washed via gentle centrifugation and resuspended in either Solution A or B (with continuous gassing as appropriate) supplemented with 1× “Complete” protease inhibitor cocktail (Roche Diagnostics Corp.). Serous cells were optically identified by size and visible morphology under DIC optics as previously described (Lee et al., 2007).

#### Simultaneous DIC Measurement of Cell Volume and Quantitative Fluorescence Measurements of pH<sub>i</sub> and [Ca<sup>2+</sup>]<sub>i</sub>

Preliminary experiments were conducted with the pH-sensitive fluorescein derivative BCECF (Molecular Probes). However, observations suggested significant cellular toxicity as a result of BCECF illumination, including abnormally high resting pH<sub>i</sub> (>7.6–7.8), rapid cytoplasmic acidification during the course of dye illumination (pH<sub>i</sub> < 7.2 after ~2–3 min of typical fluorescence sampling), and failure to observe cell shrinkage in response to CCh (as previously reported by Lee et al., 2007). Therefore, pH<sub>i</sub> measurements were instead made with SNARF-5F (Molecular Probes; Buckler and Vaughan-Jones, 1990; Liu et al., 2001). After plating on coverslips coated with Cell-Tak (BD Biosciences), isolated cells/acini were loaded with SNARF-5F by incubation in the acetoxymethyl (AM) ester derivative SNARF-5F-AM at a concentration of 5–10 µM for 10–15 min at room temperature in either Solution A or B with continuous gassing of 95% O<sub>2</sub>–5% CO<sub>2</sub> or 100% O<sub>2</sub> as appropriate. After loading, the cells adhering to the coverslip were washed via gentle pipetting of Solution A or B

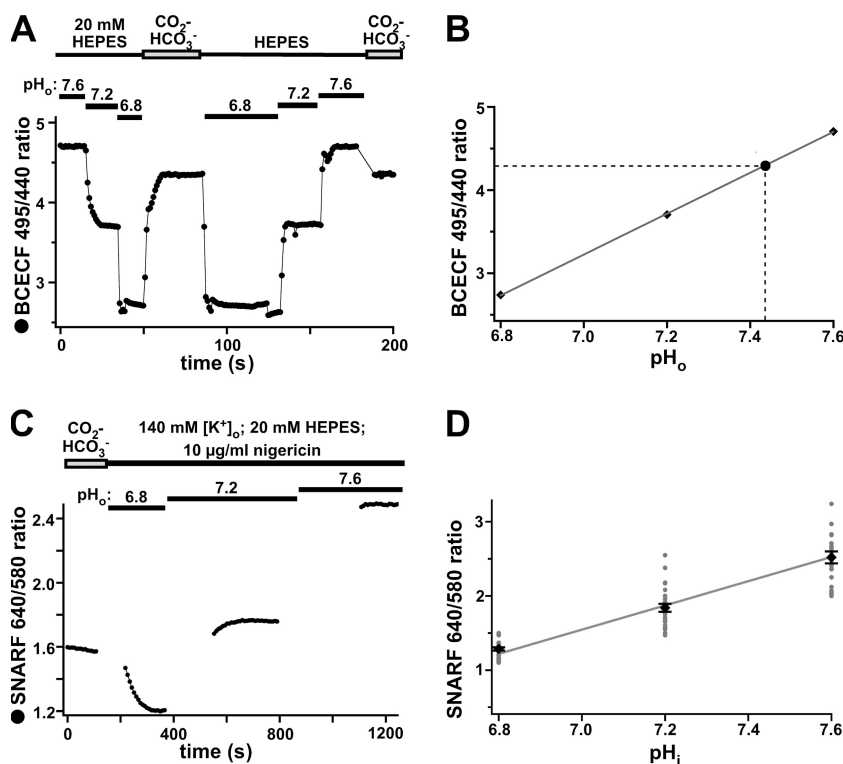


**Figure 1.** Measurement of extracellular CO<sub>2</sub>-HCO<sub>3</sub><sup>-</sup> buffer pH<sub>o</sub> and in vivo calibration SNARF pH<sub>i</sub> indicator fluorescence. (A) Measurement of pH<sub>o</sub> under experimental conditions. The experimental perfusion system was loaded with either Solution A (5% CO<sub>2</sub>-25 mM HCO<sub>3</sub><sup>-</sup>) or Solution B (HEPES with pH<sub>o</sub> = 6.8, 7.2, or 7.6 and ungassed) containing 0.5 μg/ml BCECF free acid. BCECF 495/440 nm fluorescence excitation ratios (emission collected at 535 nm) were measured upon switching between the solutions with different pH<sub>o</sub>. (B) Mean BCECF fluorescence ratios (from experiment shown in A) were plotted vs. pH<sub>o</sub> (diamonds). Mean ratios were 2.74, 3.71, and 4.71 for solutions of pH<sub>o</sub> 6.8, 7.2, and 7.6, respectively. Solid line represents linear fit to the data with slope  $2.46 \pm 0.02$  (s.d.) and intercept  $-14.0 \pm 0.2$  (s.d.). The BCECF fluorescence ratio in CO<sub>2</sub>-HCO<sub>3</sub><sup>-</sup>-buffered Solution A (large black circle) was 4.32, corresponding to pH<sub>o</sub> of  $\sim 7.44$ . (C) Example of an in vivo SNARF fluorescence calibration experiment. A SNARF-loaded serous acinar cell was treated with 10 μg/ml nigericin and exposed to 140 mM [K<sup>+</sup>]<sub>o</sub> solutions with pH<sub>o</sub> = 6.8, 7.2, and 7.6. (D) Composite calibration of SNARF 640/580 ratio measured in vivo as shown in C. Plotted are 78 raw data points (gray circles) from 26 experiments. Mean SNARF ratio values

( $\pm$ SEM; black diamonds) for pH 6.8, 7.2, and 7.6 were  $1.29 \pm 0.02$ ,  $1.84 \pm 0.05$ , and  $2.52 \pm 0.08$ , respectively. Solid line represents linear regression fit to the raw data, with slope  $= 1.6 \pm 0.1$  (s.d.) and intercept  $-9.89 \pm 0.7$  (s.d.), used to convert SNARF fluorescence ratio values to pH<sub>i</sub> values in all subsequent experiments.

(as appropriate) to remove excess unloaded dye and then incubated at room temperature for  $\sim 5$ –10 min to allow for recovery and de-esterification of loaded dye. The observed resting pH<sub>i</sub> of SNARF-loaded cells was typically stable ( $\sim 7.2$  as described below). Additionally, the rates and magnitudes of both cell shrinkage in response to CCh and cell swelling upon removal of agonist (as reported below) were nearly identical to values previously reported (Lee et al., 2007), suggesting that neither SNARF-loading nor illumination was significantly toxic to the cells over the time course of experiments ( $>20$ –40 min).

Ratiometric fluorescence measurements of pH<sub>i</sub> were performed by sequential dual-emission imaging of SNARF fluorescence collected at  $\sim 580$  and  $\sim 640$  nm. Cells were illuminated with light from a Xe arc lamp filtered through a 480/40-nm band pass (bp) filter and reflected by a 515-nm long pass (lp) dichroic to the objective lens (40 $\times$  Nikon Plan Fluor; 1.3 N.A.) for epi-illumination. Fluorescence emission collected by the objective was filtered sequentially with either a 580/10-nm bp filter or a 640/10-nm bp filter housed in a computer-controlled filter wheel (Sutter Instruments). DIC and fluorescence images were taken sequentially with a single camera using a method previously described (Foskett, 1988, 1990a) with a DIC polarizer/analyzer housed in the emission filter wheel (Lee et al., 2007). Light from a halogen lamp for DIC transillumination was filtered through a 610/10-nm bp filter and tested to ensure it did not pass through the two fluorescence emission filters or excite the SNARF dye. No measurable changes in background fluorescence and/or SNARF fluorescence were detected when high intensity 610-nm transmitted light was shuttered on and off with either the 580/10 or 640/10-nm emission filter in place. Three sequential images were taken at each time point (separated by  $\sim 250$ –500 ms): (1) SNARF fluorescence image using 480/40-nm excitation and 580/10-nm emission filters;

(2) SNARF fluorescence image using 480/40-nm excitation and 640/10-nm emission filters; (3) DIC image using filtered 610/10-nm transmitted light (Xe lamp shuttered closed) and DIC analyzer in the emission filter wheel. To minimize possible toxic effects of dye illumination, care was taken to minimize sampling frequency and both the illumination intensity (using neutral density filters) and length (exposure time) while still maintaining an acceptable signal to noise ratio (SNARF fluorescence  $>15$ -fold above background). Camera, image acquisition, and filter wheels were controlled by Perkin Elmer Ultraview LCI software.

To measure changes in [Ca<sup>2+</sup>]<sub>i</sub>, isolated serous acinar cells were loaded with 2 μM fura-2-AM (Molecular Probes) for  $\sim 10$ –15 min using a procedure similar to that described above. Simultaneous DIC imaging of cell volume and fluorescence imaging of fura-2 as well as calibration of fura-2 340/380 ratios to [Ca<sup>2+</sup>]<sub>i</sub> values were performed exactly as described previously (Lee et al., 2007). Cell volume determinations were estimated by taking the area of a DIC-imaged cross section of a serous cell or acini (traced using ImageJ software; W.S. Rasband, NIH, Bethesda, MD) to the 3/2 power, and cell volumes are expressed as normalized volumes (V) relative to the cell volume at  $t = 0$  (V<sub>o</sub>). We previously demonstrated that this method (Foskett, 1988, 1990a) provides a reproducible and accurate estimation of serous acinar cell volume when compared with cell volume measurements made via confocal 3-D reconstruction of fluorescent calcein-loaded serous cells (Lee et al., 2007).

#### Calibration of SNARF-5F in Murine Serous Acinar Cells

To quantitatively convert changes in SNARF 640/580 ratio to changes in pH<sub>i</sub>, in vivo calibration experiments were performed to calibrate the behavior of the SNARF dye in serous acinar cells. The 640/580 fluorescence emission ratios were recorded from



SNARF-loaded cells exposed to the  $H^+/K^+$  exchanger nigericin in solutions of high  $[K^+]_o$  (to equilibrate  $pH_i = pH_o$ ) with three different  $pH_o$  values (6.8, 7.2, and 7.6; example shown in Fig. 1 C). The linear regression fit of the raw data points taken from 17 calibration experiments (Fig. 1 D) was used to convert 640/580 ratios to  $pH_i$  values in all subsequent experiments. SNARF fluorescence varied linearly within the physiological  $pH_i$  range observed (Fig. 1 D).

### Measurement of Intracellular Buffering Capacity

To convert changes in  $pH_i$  to rates of base equivalent ( $OH^-$  eq) flux, cellular buffering capacity had to first be taken into account. The total intracellular acid/base buffering capacity ( $\beta_T$ ) is the sum of the  $CO_2$ - $HCO_3^-$ -dependent buffering capacity ( $\beta_{HCO_3^-}$ ) as well as the intrinsic  $CO_2$ -independent buffering capacity ( $\beta_i$ ; including  $H^+$ -buffering of cytoplasmic macromolecules and organelles). Because of marked variation in buffering capacity of various cell types (due to size and organelle composition),  $\beta_i$  must be experimentally determined. Serous acinar cell  $\beta_i$  was measured by observing  $pH_i$  changes in cells and acini exposed to solutions of various  $[NH_4Cl]_o$  in a  $Na^+$ - and  $HCO_3^-$ -free solution to block  $pH_i$  regulatory mechanisms (as previously described in Roos and Boron, 1981; Renner et al., 1989; Weintraub and Machen, 1989). It has been demonstrated that exposure of cells to a solution of  $NH_3-NH_4^+$  leads to rapid entry of membrane-permeant  $NH_3$  into the cell, causing  $pH_i$  alkalization reflective of  $H^+$  consumption as the intracellular  $NH_3$  is converted to  $NH_4^+$ . This is followed by a slower decrease in  $pH_i$ , believed to reflect  $NH_4^+$  entry, possibly through  $K^+$  channels and/or the  $Na^+/K^+$  ATPase ((Boron and De Weer, 1976; for reviews see Roos and Boron, 1981; Thomas, 1984). Upon an experimental change in  $[NH_3]_o$ , the  $[NH_4^+]_i$  can be calculated using the Henderson-Hasselbach relationship ( $[NH_4^+]_i = [NH_3]_i \times 10^{pK_a - pH_i}$ ), assuming that  $[NH_3]_i$  rapidly equilibrates with  $[NH_3]_o$  and the  $pK_a$  of intracellular and extracellular  $NH_3/NH_4^+$  is identical ( $\sim 9.2$ ; Weintraub and Machen, 1989).

Serous cells were exposed to solutions of 0, 5, 10, and 20 mM  $[NH_4Cl]_o$  (representative experiment shown in Fig. 2 A), containing 0, 0.6, 1.2, and 2.5 mM  $[NH_3]_o$ , respectively, as calculated from Henderson-Hasselbach with  $pH_o = 7.4$ . After an experimental increase or decrease in  $[NH_3]_o$ ,  $[NH_4^+]_i$  was calculated at the point of initial fast  $pH_i$  increase or decrease. The mean buffering power of all non- $NH_3-NH_4^+$ -dependent intracellular buffering (occurring around the midpoint of the  $pH_i$  change) was calculated as  $\beta_i = \Delta[NH_4^+]_i / \Delta pH_i$  (in units of mmol·liter $^{-1}$  of acid or base equivalent required to change  $pH_i$  by one unit). The raw data points taken from 24  $\beta_i$  experiments (34 imaged acini/cells; Fig. 2 B, gray circles) were then fitted with an exponential function (Fig. 2 B; solid black line; as described in the legend).

The continuously gassed 5%  $CO_2$ -95%  $O_2$ -equilibrated solution clamps  $[CO_2]_o$  constant, forming an open buffering system (for review see Roos and Boron, 1981; Boron, 2004). Because the plasma membrane is highly permeable to  $CO_2$ , it was assumed that  $[CO_2]_i = [CO_2]_o = \sim 1.2$  mM (as determined by Henry's Law with  $pCO_2 = 0.05$  atm). Using the Henderson-Hasselbach relationship and assuming that the intracellular  $pK_a$  of  $CO_2-HCO_3^-$  is  $\sim 6.1$  (Boron, 2004),  $[HCO_3^-]_i = 1.2 \text{ mM} \times 10^{pH_i - 6.1}$  and  $\beta_{HCO_3^-} = 2.3 \times [HCO_3^-]_i$  (Fig. 2 B, dashed line). Because  $[CO_2]_i$  is constant, both  $[HCO_3^-]_i$  and  $\beta_{HCO_3^-}$  rise exponentially as  $pH_i$  increases. Total intracellular pH buffering in the presence of  $CO_2-HCO_3^-$  was calculated as the sum of the two curves,  $\beta_T = \beta_i + \beta_{HCO_3^-}$  (Fig. 2 B, u-shaped solid black line). For experiments performed in the absence of  $CO_2-HCO_3^-$ , it was assumed that intracellular  $pH_i$  buffering =  $\beta_i$ .

### Measurement of $OH^-$ Equivalent and $Cl^-$ Fluxes

$OH^-$  eq flux values for each experiment were determined by first using a median-smoothing filter to minimize noise in the raw

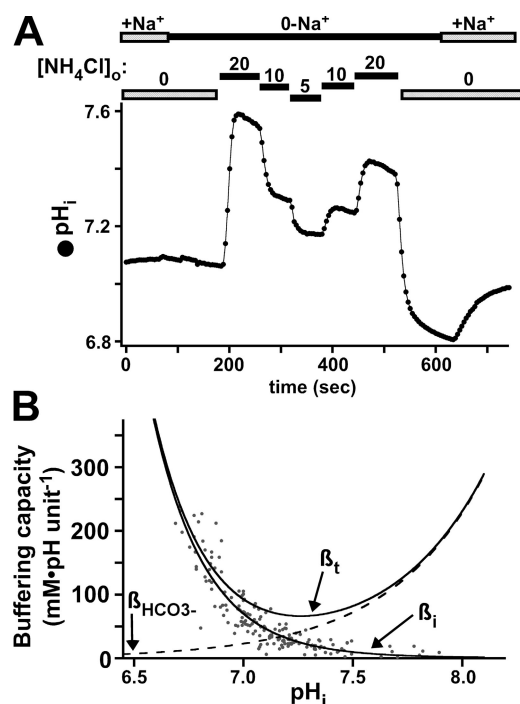


**Figure 2.** Measurement of serous acinar cell  $pH_i$  buffering capacity. (A) Representative  $NH_4Cl$  pulse experiment showing  $pH_i$  changes in response to varying  $[NH_4Cl]_o$  (from 0 to 20 mM) in  $Na^+$ - and  $HCO_3^-$ -free solution E. Intrinsic cellular buffering capacity ( $\beta_i$ ) was determined from  $NH_4Cl$ -induced  $pH_i$  changes as described in Materials and methods. (B) Measurements of serous acinar cell  $\beta_i$  plotted as a function of  $pH_i$ . Data points (circles) represent 184 measurements made in 34 separate cells/acini from experiments as shown in A. Igor Pro software was used to fit  $\beta_i$  data with an exponential function (equation of fitted line:  $\beta_i = 0.88259 + 249.8 \cdot e^{((6.69 - pH_i)/0.243)}$ ). The dashed line represents  $CO_2-HCO_3^-$ -dependent buffering ( $\beta_{HCO_3^-}$ ), calculated as  $2.3 \times [HCO_3^-]_i$  (as described in Materials and methods). The total buffering curve ( $\beta_T$ ; u-shaped curve) is the sum of the  $\beta_i$  and  $\beta_{HCO_3^-}$  curves. Conversions of changes in  $pH_i$  to  $OH^-$  eq flux values were performed using either the  $\beta_T$  or  $\beta_i$  functions in the presence or absence of  $CO_2-HCO_3^-$ , respectively.

$pH_i$  trace (Igor Pro Software; smoothing index = 3). Light median filtering best preserved the shape of the  $pH_i$  trace while removing single outlier points. The derivative of the smoothed  $pH_i$  trace was taken with respect to time (in units of pH unit·s $^{-1}$ ) for each point of the trace and then multiplied by the cellular buffering capacity (based on  $pH_i$  at that point) to obtain the  $OH^-$  eq flux (in units of meq  $OH^-$ ·liter $^{-1}$ ·s $^{-1}$ ), which was then plotted vs. time.

$Cl^-$  flux values were obtained by first converting relative cell volume values from each experiment to values of intracellular  $Cl^-$  content. As previously described (Foskett, 1990a,b, 1993), isotonic loss of cellular KCl content is reflected in a parallel decrease in  $[Cl^-]_i$  due to the presence of impermeant organic ions that make up  $>50\%$  of cellular anionic content. The linear relationship between cell volume and  $[Cl^-]_i$  in murine serous acinar cells was previously determined using the  $Cl^-$ -sensitive fluorophore SPQ (Lee et al., 2007) and described by the linear fit  $[Cl^-]_i$  (in mM)  $\approx ((V/V_o) - 0.66)/0.005$ . To determine CCh-stimulated  $Cl^-$  fluxes, the relationship between cell volume and actual  $Cl^-$  content lost by the cell was calculated from these data (i.e., the changes in cell volume must be taken into account). This transformation

TABLE II  
Primers Used for rtPCR

Transcript	GenBank/EMBL/DDBJ accession number	Expected product (bp)		Primer set (5' - 3')	5'-binding site
NHE1	NM_016981	315	for	TGTAGAGTAGAAAGTACTG	4262
			rev	TGAAAAAGGTTTCAGTTTCC	4558
NHE2	NM_001033289	127	for	CCATTTCTGTGTTTTTCCTG	3247
			rev	TCTTTAAACACTATGGGCTG	3354
NHE3	NM_001081060	207	for	AACTATGAAGAGATCAGTGG	2161
			rev	AGAGTTTGGGAATCTGAACAC	2348
NHE4	NM_177084	223	for	TTGCTCTGGAGTTTAGTAAC	3566
			rev	TATTGATCTGGTTGCCATAG	3769
NHE5	NM_001081332	356	for	TCAGGAGTAGAGAATAGTAG	4763
			rev	CCTTTGTCTAGTAAATGCTC	5099
NHE6	NM_172780	385	for	GTGAAGAAATGTGTACTACC	2163
			rev	GTTTTTCCAACAAAGGAACC	2528
NHE7	NM_177353	403	for	GTGTATGATAATCAAGAGCC	2010
			rev	GAGTGGAAGATAGTTTCAG	2384
NHE8	NM_148929	249	for	TTCTTTCTTCTCTGACATGG	4237
	NM_178371		rev	TAACATATCCAGTCATGTGAC	4466
NHE9	NM_177909	226	for	ACCTTATCACATGTATCCTC	2212
			rev	ATCCAAAATCCACATGAAGG	2418

assumed that resting  $[\text{Cl}^-]_i = \sim 65$  mM in SNARF-loaded acinar cells, as previously measured in SPQ-loaded acinar cells ( $65 \pm 4$  mM; Lee et al., 2007). The  $[\text{Cl}^-]_i$  at each point (determined by the normalized cell volume) was multiplied by the normalized cell volume. For example, at rest,  $[\text{Cl}^-]_i$  was  $\sim 65$  mM. If  $V/V_o$  falls to 0.80,  $[\text{Cl}^-]_i$  falls to  $\sim 28$  mM, but because the  $\text{Cl}^-$  is contained in a smaller volume (the cell shrunk), the change in  $[\text{Cl}^-]_i$  underestimates the actual amount of  $\text{Cl}^-$  content lost. Multiplying  $[\text{Cl}^-]_i$  (28 mM) by volume (0.80) yields a  $\text{Cl}^-$  content of 22 mmol per liter of original (resting) cell volume (i.e., the cell lost  $66 - 22 = \sim 44$  mmol  $\text{Cl}^- \cdot \text{liter}^{-1}$ ). Using the volume traces, normalized cell volume was multiplied by the  $[\text{Cl}^-]_i$  at each point, and  $\text{Cl}^-$  flux was computed by taking the derivative of the  $\text{Cl}^-$  content trace with respect to time (in units of  $\text{meq Cl}^- \cdot \text{liter}^{-1} \cdot \text{s}^{-1}$ ). Following electrophysiological convention, efflux of an anion across the plasma membrane out of a cell results in negative (inward) current, and thus negative  $\text{Cl}^-$  and  $\text{OH}^-$  eq flux values represent efflux of cellular  $\text{Cl}^-$  and  $\text{OH}^-$  equivalents.

#### Gene Expression Profiling of NHE Transcripts in Serous Acinar Cells

Gene expression profiling was performed as previously described ((Lee et al., 2007) using the method of (Van Gelder et al., 1990), for review see Eberwine, 2001). In brief, single small serous acini (three to four cells) plated on Cell-Tak-coated coverslips (washed several times to remove cellular and noncellular debris) were harvested by gentle suction with a pulled patch clamp glass electrode of  $\sim 5$   $\mu\text{m}$  diameter (taking care not to aspirate any debris). Two rounds of antisense RNA (aRNA) amplification were performed using a poly dT-oligo (to selectively amplify expressed mRNA) containing a T7 RNA polymerase promoter. Control RNA (from murine nasal turbinate, kidney, and brain) was extracted from surgically dissected tissue using TRIzol reagent (Invitrogen) according to the manufacturer's protocol. Due to the intrinsic 3'-biasing of aRNA amplification, primers were directed to the 3' end of the published transcript sequences ( $\sim 300$ –1,000 bp from the poly-A tail) obtained from GenBank/EMBL/DDBJ. Nonquantitative reverse transcription (rt)-PCR reactions were performed using a thermocycler and temperatures of 94°C, 57°C, and 72°C for

denaturation, annealing, and extension steps, respectively. Reactions were run on a 1.8% agarose gel stained with ethidium bromide and visualized on a UV light box for photography. Transcript-specific primers and expected product sizes are listed in Table II. Four serous acinar aRNA samples and three parotid acinar aRNA samples from acini harvested from three different Wt C57BL/6 mice were used in these studies, as well as kidney, brain, and nasal turbinate RNA isolated from tissue taken from two different Wt C57BL/6 mice. No differences in tissue specific NHE transcript expression were observed between the mice. As controls, PCR reactions were performed on isolated RNA in which the reverse transcription (rt) step was omitted and no PCR products were detected (not depicted), suggesting that the results were reflective of RNA expression and not contaminating genomic DNA.

#### Immunocytochemistry and Confocal Immunofluorescence Microscopy

Isolated serous acinar cells and acini were plated on glass coverslips (coated with Cell-Tak) for  $\sim 30$ –45 min in Solution B. Cells and acini were then fixed with a solution of 4% formaldehyde in Dulbecco's PBS (DPBS; w/ $\text{Ca}^{2+}$  and  $\text{Mg}^{2+}$ ; GIBCO BRL) for 20 min at room temp. Following aspiration of the fixative solution and three washes with DPBS ( $\sim 5$  min each), the coverslips were incubated for 1 h at room temp in DPBS containing 1% BSA, 1% normal goat serum, and 0.15% saponin. Primary antibody incubation was performed overnight at 4°C in the same solution. Anti-NHE1 antibody (NHE1-1A) was used at a final concentration of  $\sim 10$   $\mu\text{g}/\text{ml}$ . As a control for antibody specificity, NHE1 antigenic blocking peptide (NHE1-1P) was preincubated with 1° anti-NHE1 antibody at a concentration of 50  $\mu\text{g}/\text{ml}$  (fivefold excess by weight) for  $\sim 1$  h at 4°C. Polyclonal rabbit antiserum against NKCC1 ( $\alpha$ -wCT; directed against the C terminus of rat NKCC1; Parvin et al., 2007) was used at a 1:300 dilution. Anti-CFTR monoclonal antibody 24-1 was used at a final dilution of 1:100. The specificity of CFTR immunostaining with 24-1 was previously demonstrated by use of serous acinar cells isolated from the *cfr<sup>tm1Unc</sup>/-* mice and by inhibition of immunostaining by an antigen-containing C-terminal CFTR peptide (Lee et al., 2007).

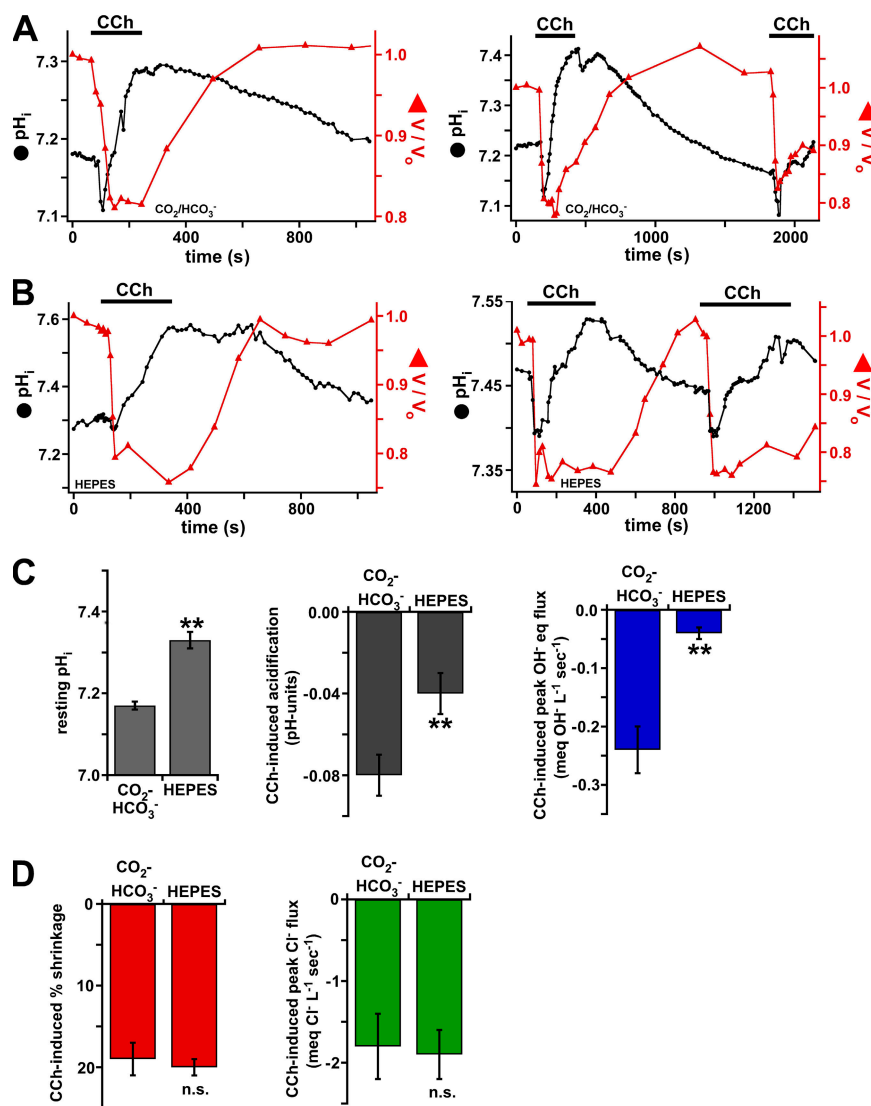


**Figure 3.** Serous acinar cell pH<sub>i</sub> responses to CCh stimulation. (A) Representative experiments showing pH<sub>i</sub> (black circles; left axes) and cell volume (red triangles; right axes) responses of SNARF-loaded serous acinar cells to stimulation with 100 μM CCh in CO<sub>2</sub>-HCO<sub>3</sub><sup>-</sup>-buffered solution, showing transient acidification occurring concomitantly with CCh-induced cell shrinkage/Cl<sup>-</sup> efflux followed by a prolonged alkalinization. Upon removal of agonist, pH<sub>i</sub> relaxed back to near resting levels. A second identical response was observed upon reapplication of agonist (second panel). (B) Representative traces from cells stimulated with CCh in nominally CO<sub>2</sub>-HCO<sub>3</sub><sup>-</sup>-free (HEPES-buffered) solution, resulting in ~50% smaller acidification (compared with CO<sub>2</sub>-HCO<sub>3</sub><sup>-</sup> conditions) but a similar subsequent pH<sub>i</sub> increase. (C) Summary of resting pH<sub>i</sub> (left), CCh-induced pH<sub>i</sub> decrease (middle), and CCh-induced OH<sup>-</sup> eq flux (right) in CO<sub>2</sub>-HCO<sub>3</sub><sup>-</sup>- and HEPES-buffered conditions. (D) Summary of cell shrinkage (left) and Cl<sup>-</sup> fluxes (right).

Following 1° antibody incubation and three subsequent washes with DPBS, the coverslips were incubated in solution containing Alexa-Fluor (AF)-labeled 2° antibody (AF488 anti-mouse IgG, AF568 anti-rabbit IgG, or both as appropriate; Molecular Probes) for ~1–2 h at room temp. After three final washes in dPBS, the coverslips were mounted on slides using Vectashield mounting medium for fluorescence (Vector Laboratories) containing 1.5 μg/ml 4',6-diamidino-2-phenylindole (DAPI). Slides were stored in the dark at 4°C and viewed on an inverted Nikon microscope equipped with a 60× (1.4 N.A.; Nikon Plan Apochromat) objective lens. Immunofluorescent staining was visualized using the 488 and 568 lines of an Ar/Kr-ion laser attached to a Perkin Elmer Ultraview LCI spinning-disc confocal system. DAPI was visualized via wide-field fluorescence microscopy by moving a filter cube (containing a 400-nm lp dichroic mirror) into the light path to reflect light from a Xe-arc lamp (filtered through a 380/10-nm bp filter) to the specimen for epi-illumination. DAPI emission was collected and filtered through a 450-nm lp filter housed in the cube and detected by the same camera used for the confocal imaging.

#### Data Analysis

All data analysis and graphing was performed using Excel or Igor Pro Software (Wavemetrics, Inc.). Data are reported as mean ±

SEM (s.e.m.) unless standard deviation (s.d.) is indicated. Image processing was performed using Perkin Elmer Ultraview Software and/or ImageJ. Statistical significance/P values were determined using Student's two-tailed *t* test. A P value of <0.05 was considered statistically significant. For all bar graphs, a single asterisk represents *P* < 0.05, a double asterisk represents *P* < 0.01, and n.s. represents no statistical significance.

## RESULTS

### CCh Stimulation of Isolated Serous Acinar Cells Causes a Transient Acidification that Is Reduced in the Absence of CO<sub>2</sub>-HCO<sub>3</sub><sup>-</sup>

Serous acinar cells loaded with the pH<sub>i</sub> probe SNARF-5F exhibited a resting pH<sub>i</sub> of 7.17 ± 0.01 (*n* = 51) in 5% CO<sub>2</sub>-25 mM HCO<sub>3</sub><sup>-</sup>-buffered medium (Solution A) that remained stable in most cells for >30–45 min of observation. Cells and acini that initially exhibited a slowly drifting or unstable pH<sub>i</sub> (~15% of cells) were allowed to equilibrate for 3–5 min without illumination. Typically, a steady-state pH<sub>i</sub> near 7.2 was observed after this

rest period, and these cells/acini were used for experiments. However, cells that did not reach a steady-state  $pH_i$  after 3–5 min (<5% of all observed cells) were discarded. No differences were observed in the responses of cells with a preliminary slight  $pH_i$  drift and an immediately stable resting  $pH_i$ .

SNARF-loaded serous acinar cells and acini stimulated with 100  $\mu$ M CCh in  $CO_2$ – $HCO_3^-$  medium exhibited a marked decrease in cell volume of  $19 \pm 2\%$  within  $70 \pm 11$  s ( $n = 9$ ) that reversed upon removal of agonist to >95% resting volume after  $310 \pm 52$  s ( $n = 9$ ; Fig. 3 A). These responses were similar to previously reported observations (Lee et al., 2007), suggesting that SNARF loading was not toxic to  $Cl^-$  efflux and influx pathways previously characterized. Additionally, CCh stimulated a transient  $pH_i$  decrease (acidification) of  $0.08 \pm 0.01$  pH units within  $49 \pm 6$  s ( $n = 9$ ) that occurred concomitantly with the cell shrinkage (Fig. 3 A). This was followed immediately by an alkalization above the resting  $pH_i$  level ( $7.35 \pm 0.02$ ;  $n = 10$ ). Upon washout of agonist,  $pH_i$  returned to near resting levels within  $500 \pm 90$  s and remained stable until subsequent restimulation (Fig. 3 A, second panel). In nominally  $CO_2$ – $HCO_3^-$ -free solution (Solution B, buffered with HEPES and gassed with 100%  $O_2$ ), the cells exhibited an alkalized resting  $pH_i$  ( $7.33 \pm 0.02$ ;  $n = 37$ ; Fig. 3, B and C), likely due to the lack of intracellular  $H^+$  formed by the reaction of dissolved  $CO_2$  with  $H_2O$  to form  $H_2CO_3$  (which dissociates to  $HCO_3^-$  and  $H^+$ ). Serous cells in  $CO_2$ – $HCO_3^-$ -free buffer exhibited a CCh-induced acidification of  $0.03 \pm 0.01$  pH units ( $n = 10$ ; Fig. 3, B and C), smaller than the acidification observed in  $CO_2$ – $HCO_3^-$  buffer ( $P < 0.01$ ). However, the time to peak acidification ( $59 \pm 9$  s) was not different. In contrast to the reduced initial acidification, the subsequent CCh-induced alkalization remained intact in the absence of  $CO_2$ – $HCO_3^-$ , as  $pH_i$  increased to  $7.47 \pm 0.05$  ( $n = 9$ ). No differences were observed in the magnitude or rate of CCh-induced cell shrinkage ( $20 \pm 1\%$  within  $74 \pm 7$  s;  $n = 8$ ) or cell swelling upon CCh removal (time to return to >95%  $V_o = 297 \pm 44$  s;  $n = 8$ ) in HEPES-buffered conditions compared with  $CO_2$ – $HCO_3^-$ -buffered conditions. These results are summarized in Fig. 3 (C and D) and suggest that  $CO_2$ – $HCO_3^-$  is required for maximal CCh-induced acidification, but not for the activation of the observed alkalization mechanism nor for either normal cell shrinkage ( $Cl^-$  efflux) or cell swelling ( $Cl^-$  influx).

Serous acinar cell buffering capacity measurements were performed to enable extrapolation of  $pH_i$  changes to magnitudes of base equivalent ( $OH^-$  eq) fluxes (Fig. 2). In  $CO_2$ – $HCO_3^-$ -containing medium, the peak net  $OH^-$  eq flux during CCh-induced acidification was  $-0.23 \pm 0.04$  meq·liter $^{-1}$ ·s $^{-1}$  ( $n = 11$ ; Fig. 3 C). This peak  $OH^-$  eq flux coincided with the peak CCh-induced net  $Cl^-$  flux of  $-1.8 \pm 0.4$  meq·liter $^{-1}$ ·s $^{-1}$  ( $n = 11$ ; Fig. 3 D). Confirming the similar kinetics of the initial CCh-induced

acidification and cell shrinkage (as shown in the traces in Fig. 3), the peak  $OH^-$  eq and  $Cl^-$  fluxes occurred concomitantly, at  $19 \pm 2$  and  $17 \pm 2$  s, respectively (n.s.), after the onset of cell shrinkage. In HEPES-buffered conditions, the initial  $OH^-$  eq flux during CCh stimulation was  $-0.04 \pm 0.01$  meq·liter $^{-1}$ ·s $^{-1}$ , equivalent to only ~19% of the flux observed in  $CO_2$ – $HCO_3^-$ -buffered conditions ( $P < 0.01$ ). In contrast, the CCh-induced peak  $Cl^-$  flux in HEPES buffer ( $-1.9 \pm 0.3$  meq·liter $^{-1}$ ·s $^{-1}$ ; Fig. 3 D) was identical to that observed in  $CO_2$ – $HCO_3^-$  buffer (n.s.). As observed in  $CO_2$ – $HCO_3^-$ , the peak CCh-induced  $Cl^-$  and  $OH^-$  eq fluxes occurred concomitantly, at  $20 \pm 4$  and  $22 \pm 4$  s, respectively, after the onset of cell shrinkage. These values were not different from each other or those observed in  $CO_2$ – $HCO_3^-$  buffer. These results demonstrate that the CCh-induced  $OH^-$  eq flux during the initial CCh-induced acidification was strongly  $CO_2$ – $HCO_3^-$ -dependent. In contrast, the  $Cl^-$  efflux underlying the CCh-induced cell shrinkage was unaffected by the presence or absence of  $CO_2$ – $HCO_3^-$ .

#### Inhibition of $Na^+/H^+$ Exchange Increases the Magnitude of and Prolongs the CCh-induced Acidification

The marked alkalization subsequent to the rapid transient CCh-induced acidification suggested that, in addition to the initial CCh-induced net  $OH^-$  eq efflux, an alkalization mechanism is also activated during CCh stimulation. The most ubiquitous cellular  $pH_i$  control mechanism is plasma membrane  $Na^+/H^+$  exchange, mediated primarily by the SLC9A family of  $Na^+/H^+$  exchange proteins (NHEs; for reviews see Orlowski and Grinstein, 2004; Zachos et al., 2005). At least 10 NHE isoforms have been cloned from mammalian cells (for review see Orlowski and Grinstein, 2004). The main plasma membrane NHE isoforms (NHE1–5 and possibly 8) are believed to operate with an electroneutral 1:1  $Na^+:H^+$  stoichiometry. NHE1 is ubiquitous, where it plays a crucial role in  $pH_i$  homeostasis (for review see Masereel et al., 2003). In addition, NHEs can have specialized roles in secretory and absorptive epithelia, including sustaining secondarily active  $Cl^-$  secretion (via basolateral NHE1 activity in concert with basolateral  $Cl^-/HCO_3^-$  [anion] exchange [AE], as observed in parotid acinar cells; Robertson and Foskett, 1994; for review see Melvin et al., 2005) and mediating  $H^+$  secretion and/or  $Na^+$  absorption (via apical NHE2 and/or NHE3 activity, as observed in the gastrointestinal tract and kidney; for review see Zachos et al., 2005). Because of their ubiquitous nature, as well as evidence that NHE activity is up-regulated upon muscarinic stimulation in exocrine acinar cells from parotid gland (Robertson and Foskett, 1994; Robertson et al., 1997; Evans et al., 1999; Park et al., 2001), pancreas (Brown et al., 2003), and sublingual mucous glands (Nguyen et al., 2000), we hypothesized that CCh-induced NHE activity mediated the sustained



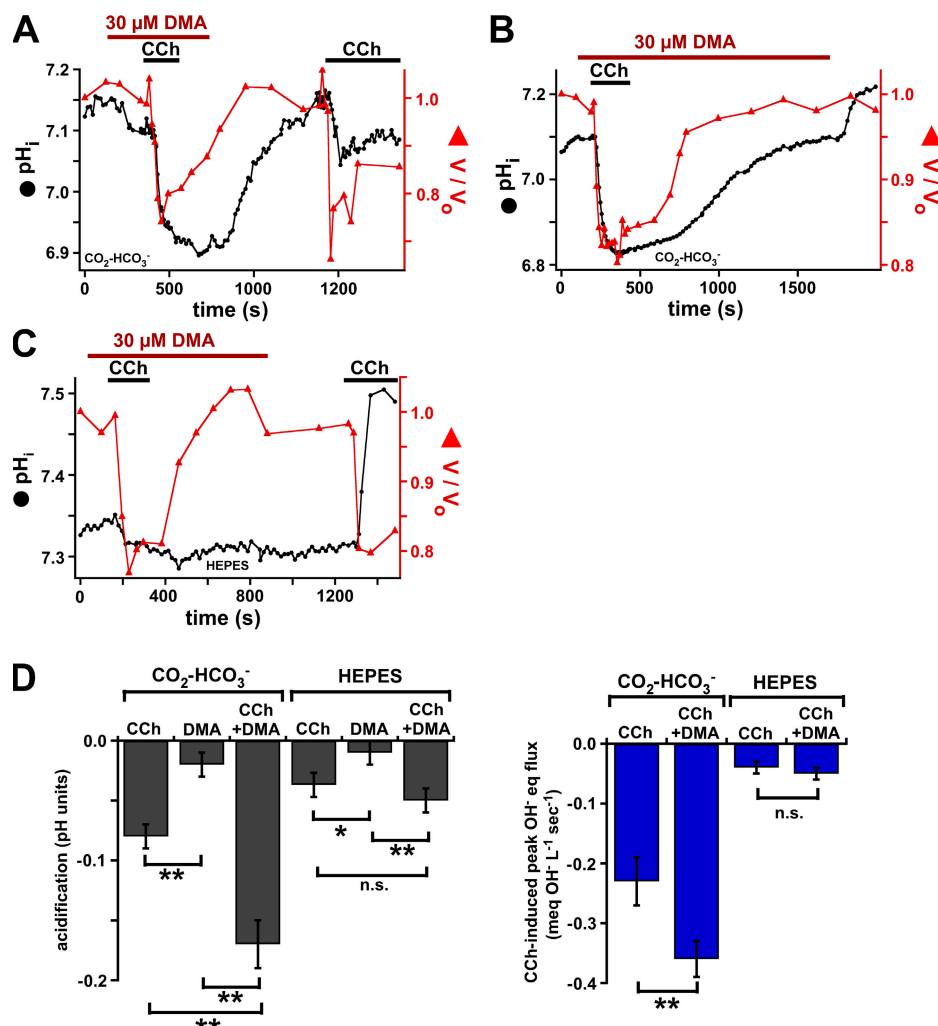


**Figure 4.** DMA enhances and prolongs CCh-induced acidification. (A) Representative experiment showing enhanced and prolonged CCh-induced acidification in serous acinar cells exposed to 30  $\mu\text{M}$  DMA in presence of  $\text{CO}_2\text{-HCO}_3^-$ . (B) After removal of CCh, 30  $\mu\text{M}$  DMA significantly slowed  $\text{pH}_i$  recovery but did not affect cell swelling ( $\text{Cl}^-$  uptake). (C) Serous cells in  $\text{CO}_2\text{-HCO}_3^-$ -free conditions stimulated with CCh in the presence of DMA exhibited small acidification nearly identical to that observed in DMA-free conditions. However, DMA strongly blocked the subsequent  $\text{pH}_i$  increase observed in presence of CCh alone. (D) Summary comparing CCh-induced acidification (left) and  $\text{OH}^-$  eq flux data (right)  $\pm$  30  $\mu\text{M}$  DMA in  $\text{CO}_2\text{-HCO}_3^-$ - and HEPES-buffered conditions.

alkalinization observed upon prolonged stimulation of serous acinar cells.

The amiloride-derivative 5-(*N,N*-dimethyl)amiloride (DMA) is a potent inhibitor of NHE activity (for review see Masereel et al., 2003). We previously showed that 30  $\mu\text{M}$  DMA (a saturating concentration for many NHE isoforms) affected neither CCh/ $\text{Ca}^{2+}$ -induced cell shrinkage ( $\text{Cl}^-$  secretion) nor cell swelling ( $\text{Cl}^-$  uptake) upon restoration of resting  $[\text{Ca}^{2+}]_i$  (Lee et al., 2007). This suggests that paired NHE/AE activity is not critical for maintenance of  $\text{Cl}^-$  secretion in airway gland serous cells, in contrast with the important role these proteins serve in sustaining parotid gland  $\text{Cl}^-$  secretion (Robertson and Foskett, 1994). The effects of DMA on agonist-induced  $\text{pH}_i$  changes were measured in SNARF-loaded serous acinar cells. Exposure of cells to 30  $\mu\text{M}$  DMA alone had little effect on resting  $\text{pH}_i$ , resulting in a maximal acidification of only  $0.02 \pm 0.01$  pH units in  $\text{CO}_2\text{-HCO}_3^-$  buffer ( $n = 6$ ) and  $0.01 \pm 0.01$  pH units in HEPES buffer ( $n = 14$ ) after prolonged ( $>300$  s) exposures. In contrast to its minimal effect on resting  $\text{pH}_i$ , DMA strongly enhanced the CCh-induced acidification

in  $\text{CO}_2\text{-HCO}_3^-$  buffer. After  $\sim 60\text{--}100$  s pretreatment with 30  $\mu\text{M}$  DMA, acinar cells were stimulated with 100  $\mu\text{M}$  CCh in the continued presence of DMA. CCh caused  $\text{pH}_i$  to drop by  $0.17 \pm 0.02$  pH units ( $n = 8$ ; Fig. 4 A, summarized in D), a greater than twofold increase compared with CCh stimulation in the absence of DMA ( $P < 0.01$ ). The peak CCh-induced  $\text{OH}^-$  eq flux in the presence of DMA ( $-0.36 \pm 0.03$  meq $\cdot\text{liter}^{-1}\cdot\text{s}^{-1}$ ;  $n = 8$ ) was also increased compared with that observed during stimulation with CCh alone ( $P < 0.05$ ; Fig. 4 D). Additionally, DMA treatment profoundly inhibited the alkalinization that typically followed the transient CCh-induced acidification (compare Fig. 4 A with Fig. 3 A) and substantially slowed  $\text{pH}_i$  recovery after removal of CCh (Fig. 4 B), as described in more detail below.

In contrast, the small CCh-induced acidification in HEPES-buffered solution was not enhanced by the presence of 30  $\mu\text{M}$  DMA ( $0.05 \pm 0.01$  pH units;  $n = 14$ ; Fig. 4 C, summarized in D). In HEPES buffer, the peak CCh-induced  $\text{OH}^-$  eq flux in the presence DMA ( $-0.05 \pm 0.01$  meq $\cdot\text{liter}^{-1}\cdot\text{s}^{-1}$ ;  $n = 14$ ) was also not different compared with that observed in the absence of DMA (summarized

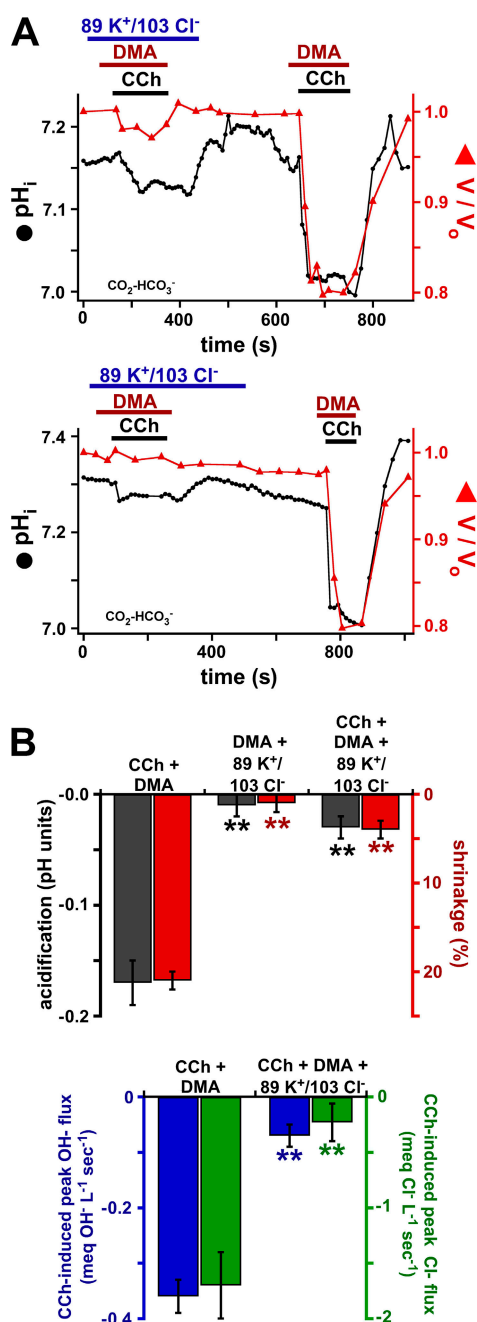


**Figure 5.** Blocking the driving force for conductive  $\text{HCO}_3^-$  efflux significantly inhibits CCh/DMA-induced acidification. (A) Representative experiments showing serous acinar cells stimulated with 100  $\mu\text{M}$  CCh after pretreatment with 30  $\mu\text{M}$  DMA in high (89 mM)  $[\text{K}^+]_o$ /low (103 mM)  $[\text{Cl}^-]_o$  conditions (Solution G), demonstrating that both cell shrinkage and acidification are blocked under these conditions. (B) Mean CCh-induced pH<sub>i</sub> decrease and cell shrinkage (top graph) along with peak CCh-induced OH<sup>-</sup> eq and Cl<sup>-</sup> fluxes (bottom graph) in Solution A (normal  $[\text{K}^+]_o$ /[ $\text{Cl}^-]_o$ ) vs. Solution G (high  $[\text{K}^+]_o$ /low  $[\text{Cl}^-]_o$ ). Asterisks represent significance when compared with 100  $\mu\text{M}$  CCh stimulation in Solution A in the presence of 30  $\mu\text{M}$  DMA.

in Fig. 4 D). However, the subsequent alkalinization observed after the transient initial CCh-induced drop (as seen in Fig. 3 B) was totally absent in the presence

of DMA (Fig. 4 B), suggesting that NHE mediates the prolonged alkalinization during CCh stimulation in the absence of  $\text{CO}_2$ - $\text{HCO}_3^-$ . In agreement with previous observations that DMA did not affect secretagogue-induced Cl<sup>-</sup> content dynamics, neither CCh-induced cell shrinkage nor the CCh-induced peak Cl<sup>-</sup> flux was affected by DMA. In  $\text{CO}_2$ - $\text{HCO}_3^-$  buffer in the presence of DMA, cells shrunk by  $21 \pm 1\%$  within  $72 \pm 11$  s with a peak Cl<sup>-</sup> flux of  $-1.7 \pm 0.3$  meq·liter<sup>-1</sup>·s<sup>-1</sup> ( $n = 8$ ), values nearly identical to those measured during CCh stimulation in the absence of DMA. The presence of DMA also had no effect on CCh-induced cell shrinkage in HEPES buffer ( $20 \pm 1\%$  within  $76 \pm 7$  s) or peak CCh-induced Cl<sup>-</sup> flux ( $-1.5 \pm 0.1$  meq·liter<sup>-1</sup>·s<sup>-1</sup>;  $n = 14$ ). DMA did not affect the similar initial kinetics of cell shrinkage and acidification in either buffer, as evidenced by the traces in Fig. 4. In  $\text{CO}_2$ - $\text{HCO}_3^-$ , the initial peak OH<sup>-</sup> eq flux and Cl<sup>-</sup> flux occurred concomitantly at  $17 \pm 5$  and  $16 \pm 3$  s, respectively, after the onset of cell shrinkage. Identical observations were made in HEPES buffer, with peak OH<sup>-</sup> and Cl<sup>-</sup> fluxes occurring at  $19 \pm 3$  and  $17 \pm 7$  s after the onset of cell shrinkage (n.s. compared with each other and compared with values in  $\text{CO}_2$ - $\text{HCO}_3^-$  buffer).

These data suggest that NHE activity is up-regulated during CCh stimulation of serous acinar cells, which minimizes the magnitude of the initial acidification present in  $\text{CO}_2$ - $\text{HCO}_3^-$ -containing medium and causes the subsequent  $\text{CO}_2$ - $\text{HCO}_3^-$ -independent alkalinization. Before further investigation of this CCh-activated NHE-mediated alkalinization (as described below), we first determined whether the initial CCh-induced net OH<sup>-</sup> eq efflux underlying the observed acidification was indeed caused by an efflux of cellular  $\text{HCO}_3^-$  content reflective of  $\text{HCO}_3^-$  secretion.

#### Reducing the Driving Force for $\text{HCO}_3^-$ Efflux Blocks CCh-induced Acidification

To test if CCh-induced acidification was caused by  $\text{HCO}_3^-$  efflux, ion substitution was used to eliminate the driving force for  $\text{HCO}_3^-$  movement, and the subsequent effects on CCh-induced pH<sub>i</sub> changes were observed. At the resting pH<sub>i</sub> of  $\sim 7.2$ , with  $[\text{HCO}_3^-]_i = \sim 16$  mM and  $[\text{HCO}_3^-]_o = 25$  mM, the Nernst equilibrium potential for  $\text{HCO}_3^-$  ( $E_{\text{HCO}_3^-}$ ) =  $\sim -12$  mV. Therefore, with the cell membrane potential ( $V_m$ ) =  $E_{\text{HCO}_3^-} = -12$  mV, the driving force for net  $\text{HCO}_3^-$  flux should be eliminated. Since stimulation of serous cells with CCh was previously shown to result in net efflux of a large quantity ( $>40$  meq liter<sup>-1</sup>) of cellular KCl (Lee et al., 2007), it was assumed that K<sup>+</sup> and Cl<sup>-</sup> permeabilities are dominant in setting  $V_m$  during CCh stimulation, and that changing  $[\text{K}^+]_o$  and  $[\text{Cl}^-]_o$  so both  $E_K$  and  $E_{\text{Cl}}$  =  $-12$  mV would clamp  $V_m$  at  $-12$  mV and abrogate the driving force for conductive  $\text{HCO}_3^-$  efflux. The mean resting  $[\text{Cl}^-]_i$  was previously determined to be  $\sim 65 \pm 4$  mM

in serous acinar cells (Lee et al., 2007). While not directly measured,  $[K^+]_i$  was assumed to be  $\sim 140$  mM, a typical  $[K^+]_i$  value as measured in other mammalian cells (for review see Foskett, 1990b). Thus under normal conditions ( $[Cl^-]_o = 135$  mM;  $[K^+]_o = 5$  mM),  $E_{Cl} = \sim -19$  mV and  $E_K = \sim -87$  mV. From the Nernst equation, it was calculated that lowering  $[Cl^-]_o$  to 103 mM and raising  $[K^+]_o$  to 89 mM would set  $E_{Cl} = E_K = E_{HCO_3^-} = -12$  mV.

Serous acinar cells were stimulated with 100  $\mu$ M CCh in the presence of 30  $\mu$ M DMA (to accentuate the observed CCh-induced acidification by blocking subsequent NHE-mediated alkalinization) in  $CO_2$ - $HCO_3^-$ -buffered solution containing 103 mM  $[Cl^-]_o$  and 89 mM  $[K^+]_o$  (Solution G; Fig. 5 A). The maximal CCh-induced acidification in high  $[K^+]_o$ /low  $[Cl^-]_o$  buffer + DMA was  $0.032 \pm 0.008$  pH units ( $n = 10$ ), and the maximal CCh-induced  $OH^-$  eq flux was  $-0.07 \pm 0.02$  meq-liter $^{-1}$ ·s $^{-1}$  ( $n = 10$ ; summarized in Fig. 5 B). These values are both  $\sim 80\%$  smaller than those observed during CCh stimulation in normal  $[K^+]_o$ /[ $Cl^-]_o$   $CO_2$ - $HCO_3^-$  buffer in the presence of DMA ( $P < 0.01$  for both). Additionally, cell shrinkage was also almost completely blocked, as expected since  $[K]_i \cdot [Cl]_i = [K]_o \cdot [Cl]_o$  and thus the driving force for KCl efflux had been nearly eliminated. Maximal CCh-induced shrinkage was reduced to  $3 \pm 1\%$  with maximal  $Cl^-$  flux of  $-0.23 \pm 0.17$  meq-liter $^{-1}$ ·s $^{-1}$  ( $n = 10$ ; summarized in Fig. 5 B). These measurements correspond to  $\sim 84\%$  and  $86\%$  inhibition, respectively, compared with observations during CCh stimulation in the presence of DMA in normal  $[K^+]_o$ /[ $Cl^-]_o$  buffer ( $P < 0.01$  for both). These results indicate that CCh-induced acidification requires conductive efflux of cellular  $HCO_3^-$ , suggesting that the acidification reflects cholinergic-stimulated  $HCO_3^-$  secretion occurring concomitantly with  $Cl^-$  secretion.

#### CFTR Is Not Required for CCh-induced Acidification

The above data demonstrate that CCh stimulation is associated with an efflux of  $HCO_3^-$  from serous acinar cells. We considered the possibility that this may occur through the same permeability that mediates the CCh-induced  $Cl^-$  efflux. We previously demonstrated that CCh-induced  $Cl^-$  efflux does not depend on CFTR, as it was not reduced in acinar cells isolated from *cftr*<sup>tm1Unc</sup> knockout mice (lacking functional CFTR; for review see Grubb and Boucher, 1999) or in acinar cells exposed to the CFTR inhibitor CFTR<sub>inh</sub>172 (Lee et al., 2007). To now examine whether CCh-induced  $HCO_3^-$  efflux requires CFTR function, we again used acinar cells isolated from the *cftr*<sup>tm1Unc</sup> mice. Acinar cells isolated from *cftr*<sup>tm1Unc</sup> mice stimulated with 100  $\mu$ M CCh in the presence of 30  $\mu$ M DMA were observed to shrink robustly ( $21 \pm 2\%$ ) with a peak CCh-induced  $Cl^-$  efflux of  $-2.2 \pm 0.2$  meq  $Cl^-$  liter $^{-1}$  s $^{-1}$  ( $n = 9$ ; unpublished data). Shrinkage was accompanied by an acidification of  $0.20 \pm$

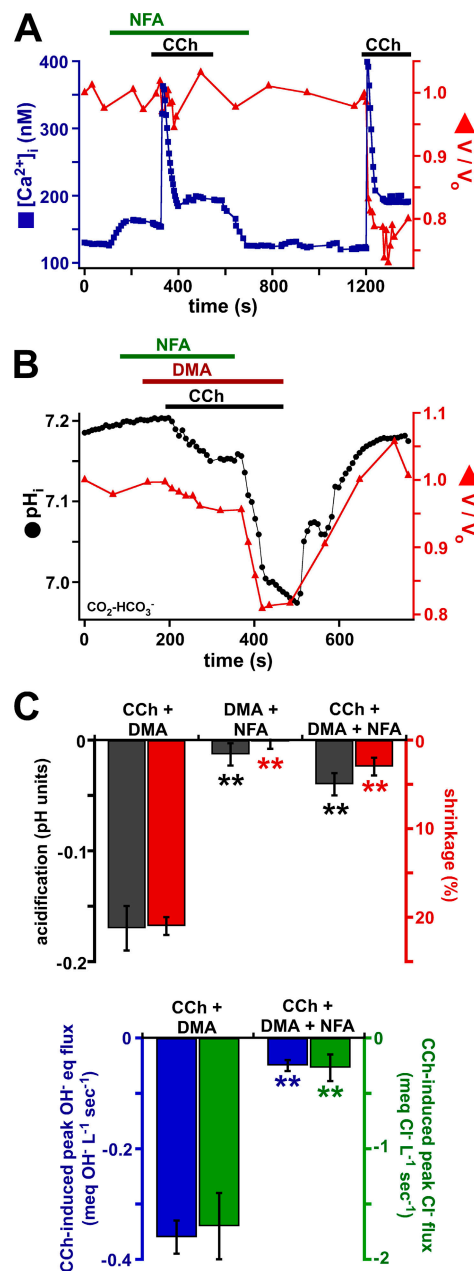


**Figure 6.** NFA inhibits CCh/DMA-induced acidification and cell shrinkage/ $Cl^-$  efflux, suggesting that both  $Cl^-$  and  $HCO_3^-$  effluxes occur through a similar  $Cl^-$  channel pathway. (A) Representative experiment showing that application of 100  $\mu$ M NFA completely blocked CCh-induced cell shrinkage/ $Cl^-$  efflux without significantly inhibiting CCh-induced  $[Ca^{2+}]_i$  signals. (B) Representative experiment showing that NFA blocks CCh-induced acidification ( $\sim 80\%$ ) in the presence of 30  $\mu$ M DMA. NFA inhibited cell shrinkage to a similar extent. (C) Summary of acidification and cell shrinkage (top) along with peak CCh-induced  $Cl^-$  and  $OH^-$  eq fluxes (bottom). Asterisks represent significance compared with 100  $\mu$ M CCh stimulation in the presence of 30  $\mu$ M DMA but in the absence of NFA.

0.02 pH units with a peak CCh-induced  $OH^-$  eq flux of  $-0.31 \pm 0.05$  meq  $OH^-$  liter $^{-1}$  s $^{-1}$  ( $n = 10$ ; unpublished data). These values were not different from those observed

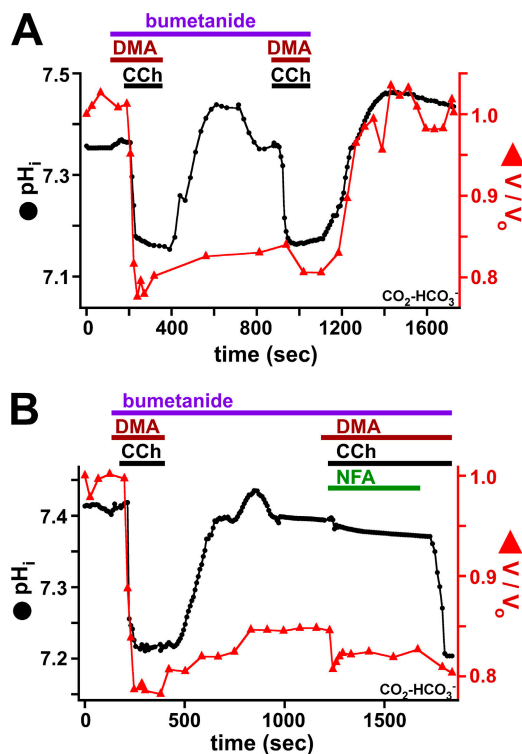


**Figure 7.** Inhibition of NKCC does not affect CCh-induced pH<sub>i</sub> dynamics, suggesting that CCh/DMA-induced acidification is not dependent on changes in [Cl<sup>-</sup>]<sub>i</sub> and that NFA block of HCO<sub>3</sub><sup>-</sup> efflux is not dependent on block of Cl<sup>-</sup> efflux. (A) Recovery of pH<sub>i</sub> after CCh + DMA-induced acidification was not dependent on influx of Cl<sup>-</sup> (cell swelling; blocked with 100 μM bumetanide). (B) Representative experiment showing NFA inhibition of CCh + DMA-induced acidification under conditions of low [Cl<sup>-</sup>]<sub>i</sub> (shrunken cell with Cl<sup>-</sup> uptake inhibited by bumetanide).

in Wt acinar cells (as reported above), suggesting that CFTR does not contribute to either the magnitude or rate of CCh-induced Cl<sup>-</sup> or HCO<sub>3</sub><sup>-</sup> efflux.

#### The Cl<sup>-</sup> Channel Blocker Niflumic Acid Strongly Inhibits both CCh-induced Cell Shrinkage/Cl<sup>-</sup> Efflux and CCh-induced Acidification/HCO<sub>3</sub><sup>-</sup> Efflux

Because CCh-induced loss of Cl<sup>-</sup> (Lee et al., 2007) or HCO<sub>3</sub><sup>-</sup> content does not depend on CFTR, we hypothesized that another Cl<sup>-</sup> channel, possibly a Ca<sup>2+</sup>-activated Cl<sup>-</sup> channel, serves as the Cl<sup>-</sup> efflux pathway during cholinergic stimulation. The nonspecific Cl<sup>-</sup> channel blocker NFA inhibits several types of heterologously expressed and endogenous Ca<sup>2+</sup>-activated Cl<sup>-</sup> currents (for review see Hartzell et al., 2005) and inhibits CCh-evoked fluid secretion from intact murine submucosal glands (Ianowski et al., 2007). We therefore examined the effects of NFA on both agonist-induced Cl<sup>-</sup> secretion and acidification. We hypothesized that NFA inhibition of the secretory Cl<sup>-</sup> channel would block agonist-induced cell shrinkage as well as OH<sup>-</sup> eq efflux. First, however, control experiments were performed to examine whether NFA interfered with CCh-triggered Ca<sup>2+</sup> signaling.

Serous cells loaded with fura-2 exhibited a 100 μM CCh-induced peak [Ca<sup>2+</sup>]<sub>i</sub> of 468 ± 57 nM followed by a plateau [Ca<sup>2+</sup>]<sub>i</sub> of 177 ± 17 nM (*n* = 10; unpublished data) in the absence of NFA (control conditions). The presence of either 10 or 100 μM NFA had no effect on these [Ca<sup>2+</sup>]<sub>i</sub> levels. The CCh-induced peak and plateau [Ca<sup>2+</sup>]<sub>i</sub> values were 397 ± 37 and 182 ± 11 nM, respectively, in the presence of 10 μM NFA (*n* = 9) and 431 ± 61 and 188 ± 60 nM, respectively, in the presence of 100 μM NFA (*n* = 5; Fig. 6 A). Nevertheless, while the CCh-induced increase in [Ca<sup>2+</sup>]<sub>i</sub> was accompanied by a 20 ± 2% shrinkage within 62 ± 8 s (*n* = 6) in the absence of NFA, the magnitude and rate of CCh/Ca<sup>2+</sup>-induced cell shrinkage was reduced to 15 ± 2% within 85 ± 6 s in the presence of 10 μM NFA (*n* = 8; *P* < 0.05 for both values). CCh-induced cell shrinkage/Cl<sup>-</sup> efflux was nearly completely inhibited with 100 μM NFA (Fig. 6 A; max shrinkage = 4 ± 2%; *n* = 5; *P* < 0.01 compared with control), despite the robust CCh-evoked [Ca<sup>2+</sup>]<sub>i</sub> response. These observations indicate that NFA blocks Cl<sup>-</sup> efflux without inhibiting the CCh/muscarinic receptor Ca<sup>2+</sup> signal, suggesting that NFA directly inhibits the secretory Cl<sup>-</sup> channel.

Exposure of acinar cells to 100 μM NFA + 30 μM DMA (to magnify any observed acidification) in the absence of CCh had little effect on either pH<sub>i</sub> or cell volume (Fig. 6 C). The maximal observed acidification was 0.01 ± 0.01 pH units and maximal observed shrinkage was 0 ± 1% (*n* = 7) after prolonged (>300 s) exposure. When acinar cells were stimulated with 100 μM CCh in the presence of both 30 μM DMA and 100 μM NFA, both cell shrinkage and acidification were severely reduced (Fig. 6 B, summarized in C). CCh caused pH<sub>i</sub> to fall by only -0.04 ± 0.01 pH units with a peak OH<sup>-</sup> eq flux of -0.05 ± 0.01 meq OH<sup>-</sup> · liter<sup>-1</sup> · s<sup>-1</sup> (*n* = 7). This corresponded to ~76% and 86% inhibition of the acidification and OH<sup>-</sup> eq flux, respectively, compared with CCh + DMA application in the absence of NFA (*P* < 0.01 for both). NFA also reduced CCh-induced cell shrinkage (4 ± 1%) and peak Cl<sup>-</sup> flux (-0.27 ± 0.12 meq Cl<sup>-</sup> · liter<sup>-1</sup> · s<sup>-1</sup>; *n* = 7). This corresponded to ~80% and ~84% inhibition, respectively, compared with CCh application in the presence of DMA alone (*P* < 0.01 for both values; summarized in Fig. 6 C). The identical magnitudes of the effects of NFA on HCO<sub>3</sub><sup>-</sup> and Cl<sup>-</sup> effluxes suggest they occur through a similar Cl<sup>-</sup> channel pathway.

#### Block of HCO<sub>3</sub><sup>-</sup> Efflux by NFA Is Not a Secondary Effect of Blocking Cl<sup>-</sup> Efflux

Another possible interpretation of the NFA inhibition of the CCh-induced acidification is that the normal fall in [Cl<sup>-</sup>]<sub>i</sub> caused by CCh stimulation provides a driving force for HCO<sub>3</sub><sup>-</sup> efflux through a Cl<sup>-</sup>/HCO<sub>3</sub><sup>-</sup> exchanger, and that NFA blocks the apparent HCO<sub>3</sub><sup>-</sup> efflux indirectly by blocking Cl<sup>-</sup> channel-mediated Cl<sup>-</sup> efflux. However, this mechanism seems unlikely due to the



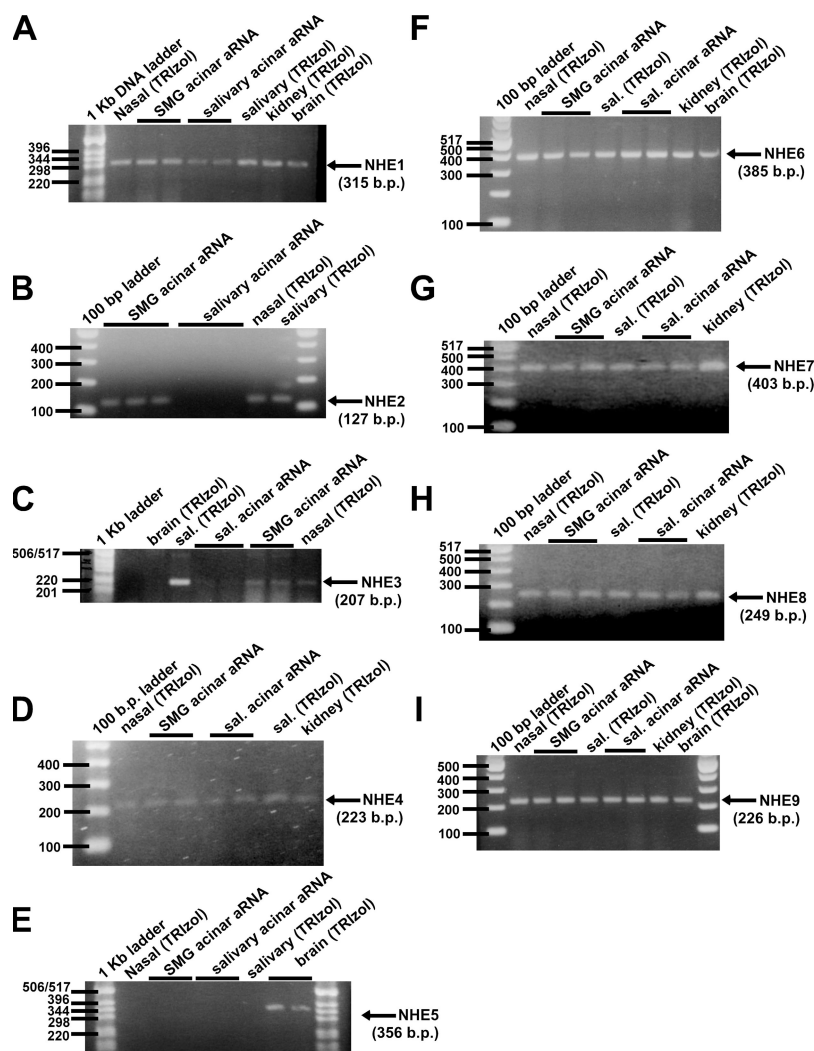


**Figure 8.** NHE isoform mRNA transcript expression in murine airway gland serous acinar cells. Messenger RNAs harvested from small airway gland serous acini were amplified and subject to rPCR using NHE isoform-specific primers (shown in Table II). (A–I) Representative EtBr-stained agarose gels showing PCR products demonstrating expression of NHE isoforms 1–9. Serous acinar cells (SMG acinar aRNA) expressed NHEs 1, 2, 3, 4, 7, 8, and 9. These isoforms were also detected in RNA isolated from nasal tissue.

reproducible kinetic correspondence of the CCh-induced acidification ( $\text{HCO}_3^-$  efflux) and cell shrinkage ( $\text{Cl}^-$  efflux). Nevertheless, to rule out a dependence of CCh-induced  $\text{OH}^-$  eq efflux on the  $\text{Cl}^-$  gradient, we examined the effect of NFA on  $\text{pH}_i$  in cells with reduced  $[\text{Cl}^-]_i$ . Serous acinar cells were stimulated with 100  $\mu\text{M}$  CCh in the presence of 30  $\mu\text{M}$  DMA and 100  $\mu\text{M}$  bumetanide (Fig. 7 A), the latter to block NKCC1-mediated  $\text{Cl}^-$  uptake (as previously shown in Lee et al., 2007). Following removal of CCh and DMA,  $\text{pH}_i$  returned to resting levels (time to 50%  $\text{pH}_i$  recovery  $190 \pm 40$  s;  $n = 4$ ), but bumetanide prevented  $\text{Cl}^-$  uptake and volume recovery. Under these conditions,  $[\text{Cl}^-]_i$  was  $\sim 30$  mM, as demonstrated previously (Lee et al., 2007). Restimulation of the shrunken  $[\text{Cl}^-]_i$ -depleted cells with CCh in the presence of 30  $\mu\text{M}$  DMA led to another acidification that was similar to that associated with the first stimulation. This second acidification was nearly completely blocked by 100  $\mu\text{M}$  NFA (Fig. 7 B; representative of three experiments), demonstrating that NFA inhibits agonist-induced acidification even under conditions of low  $[\text{Cl}^-]_i$ . These results strongly suggest that the block

of  $\text{HCO}_3^-$  efflux by NFA is a direct effect, and not a secondary effect of blocking the concomitant  $\text{Cl}^-$  efflux.

#### Expression of NHE isoform mRNA Transcripts in Serous Acinar Cells

Taken together, the above data suggest that CCh stimulation induces an acidification caused by a net loss of  $\text{OH}^-$  equivalents reflecting secretion of  $\text{HCO}_3^-$  though a  $\text{Cl}^-$  channel pathway. Because CCh also caused a prolonged DMA-sensitive alkalization following the immediate acidification, we hypothesized that NHE could function as a mechanism to maintain  $\text{HCO}_3^-$  efflux by extruding protons and alkalizing  $\text{pH}_i$  during sustained secretion (i.e., activated  $\text{Cl}^-$  and  $\text{HCO}_3^-$  efflux pathways). Because  $[\text{CO}_2]_i$  is clamped equal to  $[\text{CO}_2]_o$  as a consequence of the high membrane permeability to  $\text{CO}_2$ , this alkalization would promote the hydration of  $\text{CO}_2$  to carbonic acid, which would then dissociate to form  $\text{HCO}_3^-$  and  $\text{H}^+$  (for reviews see Roos and Boron, 1981; Boron, 2004), keeping  $[\text{HCO}_3^-]_i$  elevated. To determine which NHE isoform(s) are responsible for alkalizing  $\text{pH}_i$  during muscarinic stimulation, and whether

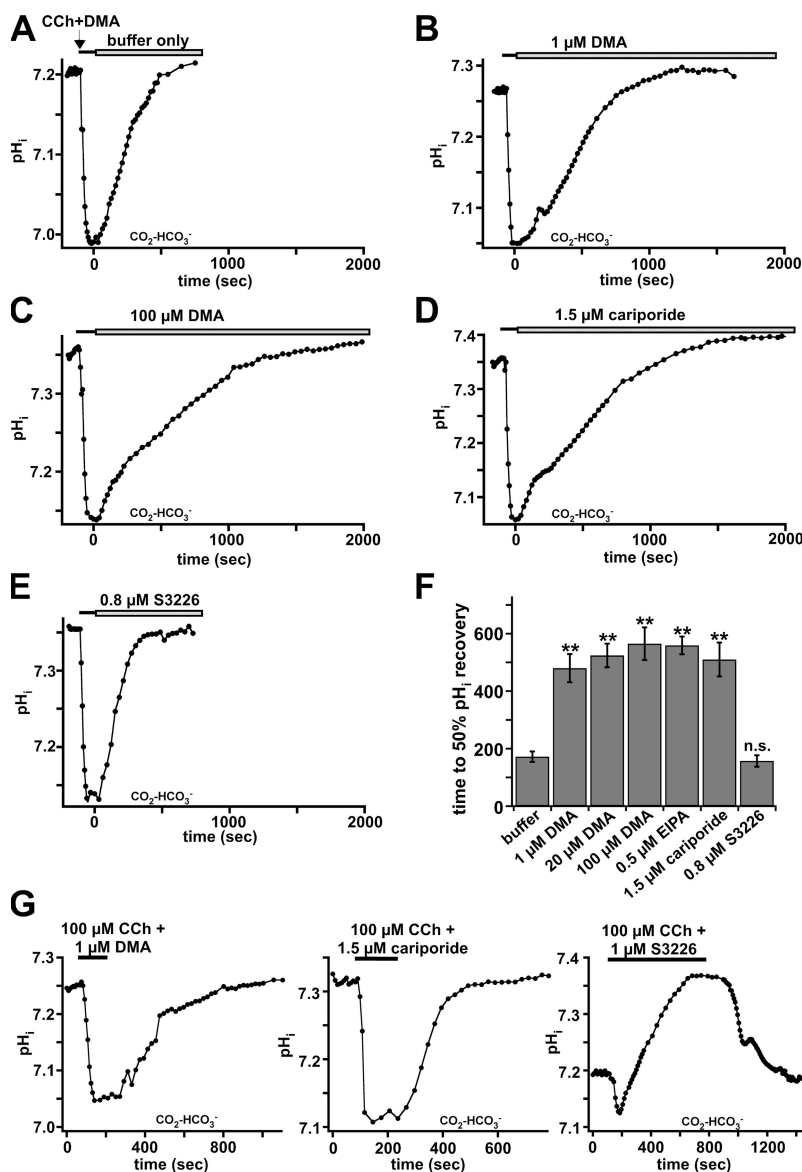


**Figure 9.** The NHE1 isoform is the major alkalinizing mechanism during CCh stimulation. (A–E) Representative experiments showing  $\text{pH}_i$  recovery (alkalinization) following acidification by 100  $\mu\text{M}$  CCh stimulation in the presence of 30  $\mu\text{M}$  DMA ( $\sim 90$  s; solid black bar) and subsequent removal of CCh and exposure to buffer only (A), 1  $\mu\text{M}$  DMA (B), 30  $\mu\text{M}$  DMA (not depicted), 100  $\mu\text{M}$  DMA (C), 0.5  $\mu\text{M}$  EIPA (not depicted), 1.5  $\mu\text{M}$  cariporide (D), or 0.8  $\mu\text{M}$  S3226 (E; open bars). Scales of x axes are identical, with the time of CCh removal set as  $t = 0$  to facilitate comparisons among experiments. All experiments performed in presence of  $\text{CO}_2\text{--HCO}_3^-$ . (F) Summary from replicate experiments as shown above. Low concentrations of DMA and EIPA (1  $\mu\text{M}$  and 0.5  $\mu\text{M}$ , respectively) and the NHE1 inhibitor cariporide inhibited alkalinization similarly to a high concentration of DMA (100  $\mu\text{M}$ ), whereas the NHE3 inhibitor S3226 had no effect. Asterisks represent significance compared with buffer only. (G) Representative experiments of serous cells stimulated with 100  $\mu\text{M}$  CCh in the presence of either 1  $\mu\text{M}$  DMA (left trace), 1.5  $\mu\text{M}$  cariporide (middle), or 1  $\mu\text{M}$  S3226 (right). Cells stimulated in presence of DMA or cariporide exhibited enhanced prolonged acidification, while cells exposed to S3226 showed only transient acidification.

this alkalinization could serve as a mechanism for sustaining  $\text{HCO}_3^-$  secretion, we used a combination of targeted gene expression profiling, pharmacology, and immunocytochemistry.

The mRNA transcript expression of various known NHE isoforms was evaluated using single-cell aRNA amplification (Van Gelder et al., 1990; for review see Eberwine, 2001) followed by reverse transcription (rt)-PCR using NHE transcript-specific primers (listed in Table II). Single small homogenous serous acini (three to four cells; as described in Materials and methods) were isolated and subject to aRNA amplification followed by rtPCR using NHE isoform-specific primers. As controls, TRIzol-extracted RNA from brain, kidney, and salivary (parotid) gland was also used, as well as RNA amplified from small parotid acini using the aRNA method. NHE1 mRNA was detected in all samples used in these studies, including aRNA amplified from small submucosal gland

serous and parotid acini (Fig. 8 A). Surprisingly, NHE2 and NHE3 transcripts were detected in RNA amplified from serous acinar cells and intact nasal turbinate tissue (Fig. 8, B and C). Neither NHE2 nor NHE3 was detected in RNA amplified from parotid acini (Fig. 8, B and C), but both transcripts were detected in RNA isolated from intact parotid gland (Fig. 8, B and C), in agreement with their expression in salivary gland ducts (Robertson et al., 1997; Park et al., 1999). As expected, NHE2 and NHE3 transcripts were detected in RNA isolated from kidney (unpublished data).

The physiological roles and expression patterns of the remaining isoforms are much less well studied. NHE4, shown to be expressed in the basolateral membranes of secretory and possibly absorptive epithelia (for review see Zachos et al., 2005), was detected in all RNA samples examined (including RNA from serous acinar cells and parotid acinar cells; Fig. 8 D). NHE5,

expressed mainly in brain (Baird et al., 1999; for review see Orłowski and Grinstein, 2004), but also in spleen, skeletal muscle (Klanke et al., 1995), and sperm (Wang et al., 2003), was not detected in any of the samples tested (including submucosal gland acinar cells) except for brain RNA (Fig. 8 E). NHE6, NHE7, NHE8, and NHE9, believed to be ubiquitous and primarily intracellular (Nakamura et al., 2005), although NHE8 may also be apically expressed in renal cortex and/or medulla (Goyal et al., 2003, 2005; Becker et al., 2007; Kang'ethe et al., 2007; Zhang et al., 2007), were detected in RNA samples isolated from nasal, parotid, and kidney tissue, as well as serous acinar cells and parotid acinar cells (Figs. 8, F–I). Neither the sperm-specific NHE isoform termed mspermNHE (Wang et al., 2003) nor the osteoclast-specific NHE10 (Lee et al., 2008) were examined here.

These gene expression data suggest that transcripts for all of the well-characterized plasma membrane isoforms thought to be involved in epithelial ion/fluid secretion and absorption (NHE1–4) were detected in serous acinar cells, in contrast to the parotid acinar cells, where only NHE1 and NHE4 were detected. The variety of plasma membrane NHEs expressed in serous cells dictated that other methods were needed to determine which of these isoform(s) was/were required for the alkalization observed during CCh stimulation.

#### The NHE1 Isoform Predominantly Contributes to Alkalization during CCh Stimulation and during $\text{pH}_i$ Recovery from CCh/DMA-induced Acidification

To elucidate the contributions of different NHE isoforms to agonist-induced alkalization in submucosal gland serous acinar cells, several NHE inhibitors were used to construct a pharmacological profile of the observed alkalization mechanism. As described above, stimulation with 100  $\mu\text{M}$  CCh in the presence of 30  $\mu\text{M}$  DMA led to an enhanced and prolonged acidification of  $\sim 0.2$  pH units. To test the effects of NHE inhibitors on  $\text{pH}_i$  recovery following this agonist-induced acidification, acinar cells were acidified by stimulation for  $\sim 90$  s with CCh in the presence of 30  $\mu\text{M}$  DMA (as shown in Fig. 9, A–E, solid black bars), followed by removal of CCh and exposure of the cells to different concentrations of DMA or other NHE inhibitors (Fig. 9, A–E, open bars). Upon removal of both CCh and DMA (“buffer only” conditions),  $\text{pH}_i$  rapidly alkalized to resting levels (time for recovery to 50% resting  $\text{pH}_i = 172 \pm 17$  s,  $n = 7$ ; Fig. 9 A). However, when CCh was removed and cells were exposed to a low concentration of DMA (1  $\mu\text{M}$ ; Fig. 9, B and F),  $\text{pH}_i$  recovery was slowed by  $>2.5$ -fold. The time to 50%  $\text{pH}_i$  recovery in the presence of 1  $\mu\text{M}$  DMA was  $480 \pm 49$  s ( $n = 4$ ;  $P < 0.01$  compared with buffer only). The time for the return to 50% of resting  $\text{pH}_i$  in the presence of 30  $\mu\text{M}$  DMA ( $524 \pm 41$  s;  $n = 7$ ; Fig. 9 F) was also slower than the recovery observed in the presence of buffer alone ( $P < 0.01$ ), but not enhanced (n.s.)

beyond that observed in the presence of 1  $\mu\text{M}$  DMA. A higher concentration of DMA (100  $\mu\text{M}$ ; Fig. 9, C and F) also increased the time to 50%  $\text{pH}_i$  recovery ( $565 \pm 57$  s,  $n = 4$ ) compared with buffer alone ( $P < 0.01$ ). However, the inhibition observed with 100  $\mu\text{M}$  DMA was not increased beyond that observed with 30  $\mu\text{M}$  DMA. These data are summarized in Fig. 9 F, and demonstrate that 1  $\mu\text{M}$  DMA is a near-saturating concentration. Reported  $\text{IC}_{50}$  values (in  $\mu\text{M}$ ) of DMA for NHE1, 2, and 3 are  $\sim 0.023$ , 0.25, and 14, respectively (for review see Masereel et al., 2003). The lack of enhanced inhibition with  $[\text{DMA}] > 1$   $\mu\text{M}$  suggests that DMA-sensitive alkalization is mediated by NHE1 and/or 2, typically classified as the “amiloride-sensitive” isoforms (for reviews see Masereel et al., 2003; Zachos et al., 2005). In agreement, a low concentration of another amiloride derivative, 5-(*N*-ethyl-*N*-isopropyl)amiloride (EIPA; 0.5  $\mu\text{M}$ ) also slowed  $\text{pH}_i$  recovery (trace not depicted, summarized in Fig. 9 F;  $559 \pm 31$  s to 50%  $\text{pH}_i$  recovery,  $n = 5$ ) compared with buffer only ( $P < 0.01$ ). The inhibition of  $\text{pH}_i$  recovery with 0.5  $\mu\text{M}$  EIPA was nearly identical to the inhibition observed with 30  $\mu\text{M}$  DMA (n.s.). EIPA has  $\text{IC}_{50}$  values (in  $\mu\text{M}$ ) of 0.01, 0.08, 2.4, and 2.5–10 for NHEs 1, 2, 3, and 4, respectively (Chambrey et al., 1997, 2001; Masereel et al., 2003). The strong inhibition observed with 1  $\mu\text{M}$  DMA and 0.5  $\mu\text{M}$  EIPA suggests that the DMA-sensitive component of the observed alkalization is mainly due to the contributions of NHE1 and/or NHE2.

To further confirm the identity of the isoform(s) involved, we used the benzoylguanidine inhibitor cariporide (HOE 642), a strongly potent and selective NHE1 inhibitor. Previously reported  $\text{IC}_{50}$  values for cariporide are (in  $\mu\text{M}$ )  $\sim 0.03$  for NHE1, 4.3 for NHE2,  $>100$  for NHE3 (Masereel et al., 2003), and  $>500$  for NHE4 (Chambrey et al., 2001). A low dose of cariporide (1.5  $\mu\text{M}$ ) strongly inhibited  $\text{pH}_i$  recovery after CCh + DMA-induced acidification (Fig. 9, D and F; time to recovery to 50%  $\text{pH}_i = 511 \pm 59$  s,  $n = 7$ ;  $P < 0.01$  compared with buffer only). This was not different than the inhibition observed with 30  $\mu\text{M}$  DMA (n.s.). In marked contrast, a low dose (0.8  $\mu\text{M}$ ) of the specific NHE3 inhibitor S3226 showed no inhibition of  $\text{pH}_i$  recovery after CCh + DMA-induced acidification (Fig. 9, E and F; time to return to 50% resting  $\text{pH}_i = 157 \pm 20$  s,  $n = 5$ ). The  $\text{IC}_{50}$  value for S3226 is 0.02  $\mu\text{M}$  for NHE3, compared with 3.6  $\mu\text{M}$  for NHE1 and  $\sim 80$   $\mu\text{M}$  for NHE2 (Schwark et al., 1998). Taken together, these data suggest that NHE1 is the primary NHE isoform contributing to  $\text{pH}_i$  recovery after CCh + 30  $\mu\text{M}$  DMA-induced acidification.

In a separate experimental protocol, serous acinar cells were stimulated with 100  $\mu\text{M}$  CCh in the presence of a low dose of DMA (1  $\mu\text{M}$ ), cariporide (1.5  $\mu\text{M}$ ), or S3226 (1  $\mu\text{M}$ ). In the presence of DMA or cariporide, a sustained and enhanced acidification was observed (Fig. 9 G, first and second panels). The CCh-induced acidification was  $0.20 \pm 0.03$  U with 1  $\mu\text{M}$  DMA ( $n = 3$ )



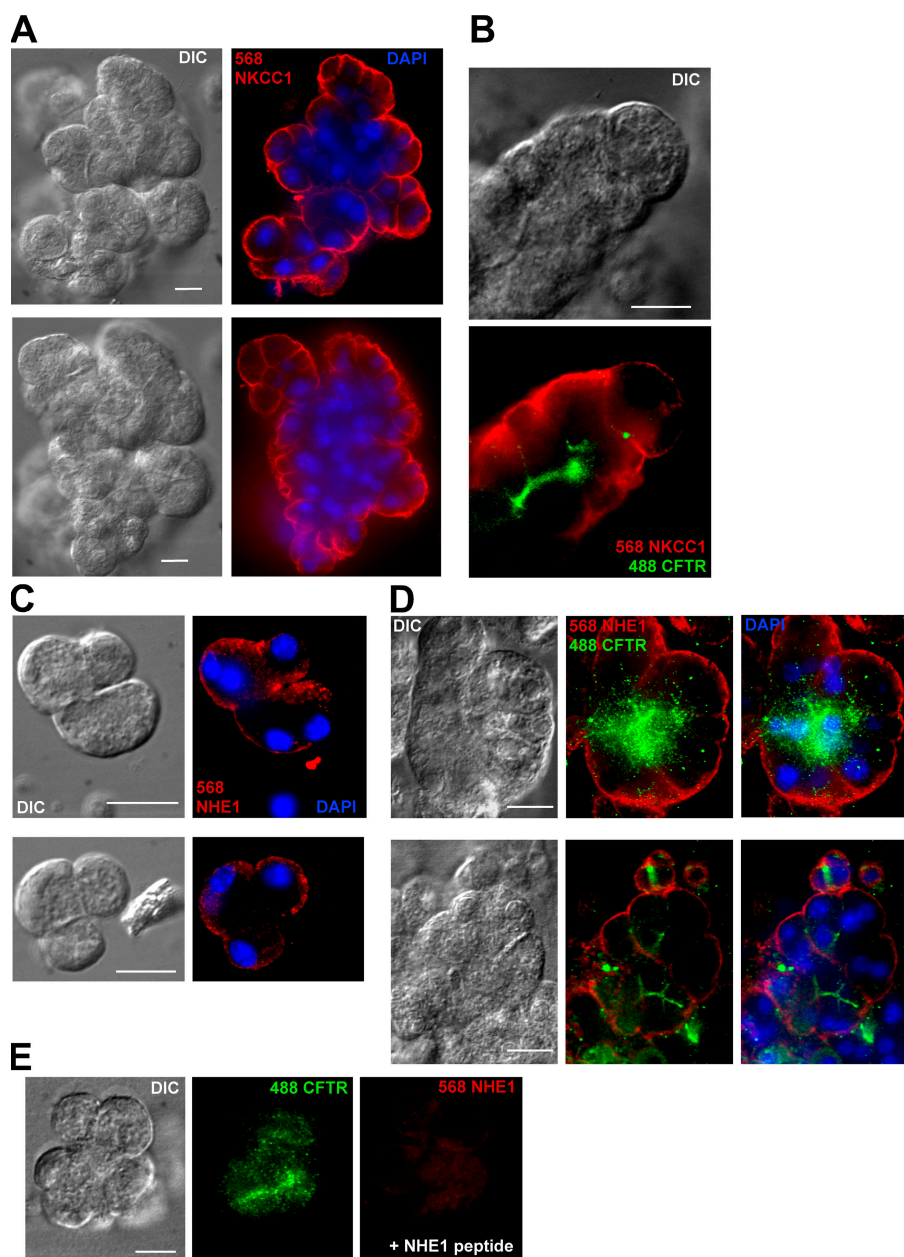


**Figure 10.** Confocal immunofluorescence microscopy indicates that NHE1 localizes to the basolateral membrane of serous acinar cells and acini. (A) Isolated, fixed serous acini exhibited NKCC1 immunofluorescence localized to the basolateral membranes. Top and bottom panels represent two separate focal planes imaged through same acinus. (B) Basolateral NKCC1 immunofluorescence did not overlap with CFTR, shown previously to be an apical serous cell marker. (C) NHE1 immunostaining revealed basolateral immunofluorescence pattern similar to that for NKCC1. (D) NHE1 immunofluorescence did not overlap with CFTR immunofluorescence. (E) Preincubation of NHE1 antibody with antigenic peptide reduced NHE1 immunofluorescence. Micrographs in E taken with identical system settings (filters, camera gain, exposure time, laser power) as used for images in D. Scale bar in each micrograph represents 10  $\mu$ m.

and  $0.21 \pm 0.03$  U with 1.5  $\mu$ M cariporide ( $n = 4$ ). This CCh-induced acidification was increased compared with that observed during stimulation with CCh alone ( $P < 0.01$ ) but was identical to that observed during CCh stimulation in the presence of 30  $\mu$ M DMA (n.s.). However, 100  $\mu$ M CCh in the presence of 1  $\mu$ M S3226 (Fig. 9 G, third panel) caused only a transient acidification ( $0.05 \pm 0.01$  units;  $n = 8$ ) that was not different from that observed during stimulation with CCh alone (n.s.) but less than the acidification observed during CCh stimulation in the presence of 1  $\mu$ M DMA ( $P < 0.01$ ) or 1.5  $\mu$ M cariporide ( $P < 0.01$ ). Taken together, these data suggest that NHE1 is the major NHE isoform that contributes to alkalinization of  $pH_i$  during conditions of CCh stimulation.

#### NHE1 Is Expressed on the Basolateral Membrane of Serous Acinar Cells

For the observed CCh-induced NHE1 activity to indeed serve as a mechanism for sustaining  $HCO_3^-$  secretion, NHE1 expression must be localized to the basolateral membrane of the serous epithelium. If NHE1 were instead localized to the apical membrane,  $HCO_3^-$  secretion would be neutralized by the parallel efflux of  $H^+$  into the acinar lumen. The localization of NHE1 was investigated by confocal immunofluorescence microscopy of isolated fixed acini and acinar cells using a polyclonal antibody against NHE1. As a control, immunostaining was also performed using a polyclonal antibody to NKCC1, a well-characterized protein expressed on the basolateral membrane of secretory epithelia (for reviews



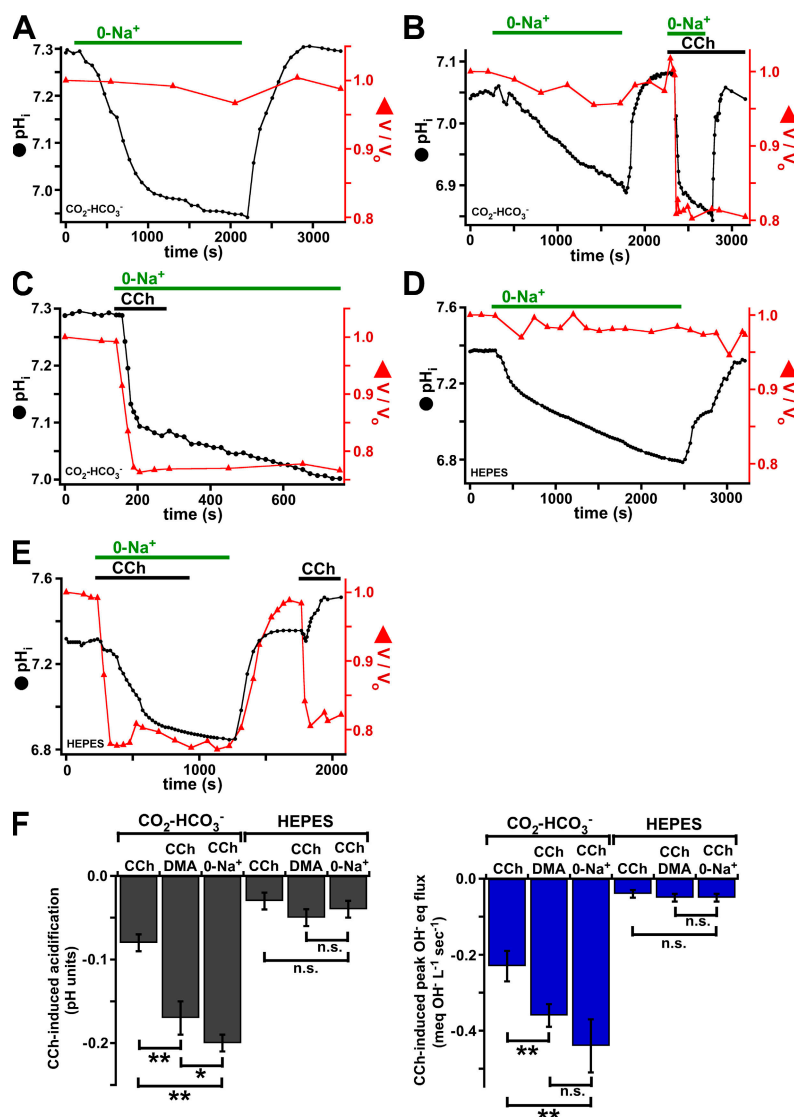


**Figure 11.** Removal of Na<sup>+</sup> enhances CCh-induced acidification and completely blocks pH<sub>i</sub> recovery. Representative experiments illustrating dependence of serous cell pH<sub>i</sub> on Na<sup>+</sup>. (A) Removal of Na<sup>+</sup> (0 Na<sup>+</sup>) in CO<sub>2</sub>-HCO<sub>3</sub><sup>-</sup> (Solution C) caused slow acidification. Cells recovered to near resting pH<sub>i</sub> upon reintroduction of Na<sup>+</sup>. (B) Stimulation of acinar cells with 100 μM CCh in 0 Na<sup>+</sup> solution elicited enhanced acidification compared with 0 Na<sup>+</sup> alone or CCh alone. (C) Cells stimulated with CCh in 0 Na<sup>+</sup> exhibited slow, progressive acidification following immediate rapid CCh-induced acidification, and lacked pH<sub>i</sub> or volume recovery upon removal of CCh. (D) Removal of Na<sup>+</sup> in HEPES buffer (Solution D) also caused prolonged acidification, with realkalinization upon reintroduction of Na<sup>+</sup>. (E) CCh stimulation in HEPES-buffered 0 Na<sup>+</sup> solution enhanced CCh-induced acidification, but to a smaller extent than observed in CO<sub>2</sub>-HCO<sub>3</sub><sup>-</sup> buffer. (F) Summary of CCh-induced acidification (left) and peak OH<sup>-</sup> eq fluxes (right) in Na<sup>+</sup>-containing and 0 Na<sup>+</sup> CO<sub>2</sub>-HCO<sub>3</sub><sup>-</sup> and HEPES buffers.

see Gerelsaikh and Turner, 2000; Haas and Forbush, 2000). Strong NKCC1 immunofluorescence was detected along apparent basal and lateral membranes of serous acini (Fig. 10 A), in agreement with functional and genetic evidence of NKCC1 expression in murine serous acinar cells (Lee et al., 2007), and functional data suggesting NKCC contributes to CCh-induced fluid secretion from intact murine submucosal glands (Ianowski et al., 2007). NKCC1 immunofluorescence did not overlap with immunofluorescence for CFTR (Fig. 10 B), previously shown to be expressed apically in serous acini (Engelhardt et al., 1992; Jacquot et al., 1993; Lee et al., 2007). The distinct patterns of NKCC1 and CFTR immunostaining support the basolateral localization of the NKCC1 immunofluorescence pattern. A similar basolateral immunofluorescence pattern was observed for NHE1 (Fig. 10 C). NHE1 immunofluorescence also did not overlap with CFTR immunofluorescence (Fig. 10 D). When NHE1 antibody was preincubated with excess antigenic peptide, NHE1 immunofluorescence was

significantly reduced while CFTR immunofluorescence was unaffected (Fig. 10 E), supporting the specificity of the NHE1 immunostaining. These data indicate that the basolateral membrane is the major site of NKCC1 and NHE1 expression in serous acinar cells, consistent with the hypothesis that NHE1 plays a crucial role in HCO<sub>3</sub><sup>-</sup> secretion during CCh stimulation.

#### Removal of Extracellular Na<sup>+</sup> Leads to a Slow Prolonged Acidification and Completely Inhibits pH<sub>i</sub> Recovery after CCh-induced Acidification, but Does Not Significantly Enhance the Initial CCh-induced OH<sup>-</sup> Eq Flux

The above data suggest that NHE1 is the main NHE isoform contributing to alkalinization during CCh-stimulated fluid secretion and during pH<sub>i</sub> recovery from CCh-induced acidification, and suggest that NHE1 localization would permit it to function in maintaining HCO<sub>3</sub><sup>-</sup> secretion. However, other pH<sub>i</sub> regulatory mechanisms exist in serous acinar cells, as evidenced by the ability of cells to alkalinize, albeit very slowly, in the presence of

100  $\mu\text{M}$  DMA. It is possible that  $\text{Na}^+$ -linked DMA-insensitive transporters, for example  $\text{Na}^+$ - $\text{HCO}_3^-$  cotransporters (NBCs), may be involved. The  $\text{Na}^+$  dependence of both resting  $\text{pH}_i$  regulation and  $\text{pH}_i$  recovery after CCh-induced acidification was evaluated using 0  $\text{Na}^+$  solutions ( $\text{Na}^+$  isosmotically replaced by NMDG $^+$ ). In  $\text{CO}_2$ - $\text{HCO}_3^-$ -buffered conditions, removal of  $\text{Na}^+$  from the extracellular medium led to a continuous acidification (Fig. 11 A), suggesting that  $\text{Na}^+$  is required for regulation of resting  $\text{pH}_i$ . The acidification was slow ( $0.01 \pm 0.003$  pH unit $\cdot\text{min}^{-1}$  during the first 10 min of observation), with a maximal net  $\text{OH}^-$  eq flux of  $-0.04 \pm 0.01$  meq  $\text{OH}^- \cdot \text{liter}^{-1} \cdot \text{min}^{-1}$  ( $n = 6$ ). CCh stimulation in 0  $\text{Na}^+$   $\text{CO}_2$ - $\text{HCO}_3^-$  buffer (Fig. 11, B and C) caused an immediate fast drop in  $\text{pH}_i$  of  $0.20 \pm 0.01$  U ( $n = 8$ ). This was  $\sim 2.5$ -fold larger than the acidification observed with CCh stimulation in normal  $\text{Na}^+$ -containing  $\text{CO}_2$ - $\text{HCO}_3^-$  buffer ( $P < 0.01$ ) and also slightly larger than that observed with CCh stimulation in  $\text{Na}^+$ -containing  $\text{CO}_2$ - $\text{HCO}_3^-$  buffer in the presence of 30  $\mu\text{M}$  DMA ( $P < 0.05$ ). The peak CCh-induced  $\text{OH}^-$  eq flux in  $\text{Na}^+$ -free  $\text{CO}_2$ - $\text{HCO}_3^-$  buffer was  $-0.44 \pm 0.07$  meq  $\text{OH}^- \cdot \text{liter}^{-1} \cdot \text{s}^{-1}$  ( $n = 8$ ). This value was approximately twofold larger than that observed with CCh stimulation in  $\text{Na}^+$ -containing  $\text{CO}_2$ - $\text{HCO}_3^-$  buffer ( $P < 0.01$ ) but nearly identical to that observed during CCh stimulation in  $\text{Na}^+$ -containing  $\text{CO}_2$ - $\text{HCO}_3^-$  buffer in the presence of 30  $\mu\text{M}$  DMA (n.s.). CCh-induced acidification and  $\text{OH}^-$  eq flux values are summarized in Fig. 11 F.

The fact that CCh-induced  $\text{OH}^-$  eq efflux and acidification in 0  $\text{Na}^+$  solution were only slightly enhanced compared with those observed in  $\text{Na}^+$ -containing solution with saturating [DMA] strongly suggests that NHE1 is the major alkalizing mechanism activated during CCh stimulation. However, the slow alkalization mechanisms observed in cells stimulated with CCh in the presence of DMA were absent in cells stimulated with CCh in 0  $\text{Na}^+$  buffer, as cells continued to acidify after the initial CCh-induced drop (Fig. 11 C) regardless of whether CCh was removed. The complete lack of  $\text{pH}_i$  recovery in 0  $\text{Na}^+$  solution suggests that the DMA-insensitive  $\text{pH}_i$  recovery mechanism(s) observed in the cells are strongly dependent upon extracellular  $\text{Na}^+$ . In contrast, 0  $\text{Na}^+$  conditions did not affect CCh-induced cell shrinkage ( $23 \pm 1\%$ ) or maximal  $\text{Cl}^-$  flux rate ( $-1.7 \pm 0.2$  meq $\cdot\text{Cl}^- \cdot \text{liter}^{-1} \cdot \text{s}^{-1}$ ;  $n = 8$ ) compared with CCh stimulation in  $\text{Na}^+$ -containing buffer (n.s.). However, cell swelling upon removal of CCh was completely blocked in 0  $\text{Na}^+$  conditions (Fig. 11 C), likely due to total inhibition of NKCC1.

In the absence of  $\text{CO}_2$ - $\text{HCO}_3^-$ , removal of  $\text{Na}^+$  (0  $\text{Na}^+$  Solution D; Fig. 11 D) also caused  $\text{pH}_i$  to fall ( $-0.03 \pm 0.01$  pH unit $\cdot\text{min}^{-1}$  during the first 10 min of observation), faster than that observed under 0  $\text{Na}^+$  conditions in the presence of  $\text{CO}_2$ - $\text{HCO}_3^-$  ( $P < 0.05$ ). However, this apparent increased rate was due to the reduced buffer-

ing capacity of cells lacking  $\beta_{\text{HCO}_3^-}$ , as the peak net  $\text{OH}^-$  eq flux ( $-0.05 \pm 0.02$  meq  $\text{OH}^- \cdot \text{liter}^{-1} \cdot \text{min}^{-1}$ ;  $n = 7$ ) was not increased beyond that observed in 0  $\text{Na}^+$   $\text{CO}_2$ - $\text{HCO}_3^-$  buffer (n.s.). The initial CCh-induced acidification ( $0.04 \pm 0.01$  pH units) and  $\text{OH}^-$  eq flux values ( $-0.05 \pm 0.01$  meq  $\text{OH}^- \cdot \text{liter}^{-1} \cdot \text{min}^{-1}$ ;  $n = 5$ ) in 0  $\text{Na}^+$  HEPES-buffered solution were identical to those observed during CCh stimulation in  $\text{Na}^+$ -containing HEPES buffer (n.s.). However, the CCh-induced acidification and  $\text{OH}^-$  eq flux values in 0  $\text{Na}^+$  HEPES buffer were only  $\sim 25\%$  and  $\sim 12\%$ , respectively, of those observed in 0  $\text{Na}^+$   $\text{CO}_2$ - $\text{HCO}_3^-$  buffer ( $P < 0.01$  for both; Fig. 11, E and F). Nevertheless, as observed in  $\text{CO}_2$ - $\text{HCO}_3^-$  buffer, cells exhibited no ability to recover either  $\text{pH}_i$  or cell volume under  $\text{Na}^+$ -free  $\text{CO}_2$ - $\text{HCO}_3^-$ -free conditions (Fig. 11 E), as  $\text{pH}_i$  continued to acidify for  $>30$  min of observation. Taken together, these data suggest that DMA-insensitive  $\text{Na}^+$ -dependent  $\text{pH}_i$  regulatory mechanisms are involved in maintenance of resting  $\text{pH}_i$  and full recovery after agonist-induced acidification.

## DISCUSSION

### Serous Acinar Cells Secrete $\text{HCO}_3^-$ in Response to Muscarinic Stimulation

Exocrine gland fluid secretion is mediated by a complex set of ion channels and transporters acting in concert and subject to intricate feedback and regulatory mechanisms (for review see Melvin et al., 2005). The generalized model of epithelial fluid secretion dictates that secondarily active basolateral transport (coupled to the  $\text{Na}^+$  gradient and membrane potential generated by the  $\text{Na}^+/\text{K}^+$  ATPase) leads to accumulation of anions ( $\text{Cl}^-$ ,  $\text{HCO}_3^-$ ) inside the secretory cell at concentrations above their electrochemical equilibrium. During secretion, these anions can exit across the apical membrane, with basolateral  $\text{K}^+$  channels allowing for efflux of  $\text{K}^+$  and maintenance of electroneutrality. The resulting negative transepithelial potential draws  $\text{Na}^+$  across the epithelium, likely through a paracellular pathway, and osmotically obliged water follows the movement of the  $\text{Na}^+$  and  $\text{Cl}^-$  ions. We previously examined the mechanisms of fluid secretion in airway submucosal gland serous acinar cells from murine nasal tissues, by imaging agonist-induced cell volume changes to track changes in cell solute content, along with fluorescence microscopy of ion indicator dyes (Lee et al., 2007). Serous cells stimulated with CCh shrank by  $\sim 20\%$  in response to a muscarinic-induced increase in  $[\text{Ca}^{2+}]_i$  and stimulation of  $\text{Ca}^{2+}$ -activated membrane permeabilities. Cell shrinkage was caused by efflux of  $>60\%$  of cell  $\text{Cl}^-$  content associated with activation of  $\text{Cl}^-$  secretion. Sustained  $\text{Cl}^-$  secretion required the activity of the NKCC1 cotransporter, with no apparent involvement of coupled  $\text{Na}^+/\text{H}^+$  and  $\text{Cl}^-/\text{HCO}_3^-$  exchangers.

In this study, the capacity of acinar cells to secrete  $\text{HCO}_3^-$  was evaluated. We performed quantitative measurements of  $\text{pH}_i$  at rest and during cholinergic stimulation. Because changes in cell volume provide information regarding the fluid secretory state of the cells, cell volume was measured simultaneously with  $\text{pH}_i$ . Our results indicate that cholinergic stimulation of fluid secretion is associated with activation of two major mechanisms that acidify and alkalinize the cells, respectively, that together mediate  $\text{HCO}_3^-$  secretion. Several pieces of evidence suggest that the initial rapid acidification was caused predominately by  $\text{HCO}_3^-$  efflux. First, the magnitude of the acidification was greatly enhanced by the presence of  $\text{CO}_2\text{--HCO}_3^-$  in the medium. This was particularly evident when activation-induced alkalinization mechanisms ( $\text{Na}^+/\text{H}^+$  exchange) were inhibited. Importantly, elimination of the electrochemical driving force for conductive  $\text{HCO}_3^-$  efflux (clamping  $V_m = E_{\text{HCO}_3^-}$ ) by manipulation of the concentrations of  $\text{K}^+$  and  $\text{Cl}^-$ , the two major ions that determine membrane potential in acinar cells, nearly completely eliminated the acidification. This result suggests that the acidification is mediated by  $\text{HCO}_3^-$  efflux, and furthermore that the efflux mechanism is conductive.

#### The Nature of the $\text{HCO}_3^-$ Efflux Pathway

The kinetics of the agonist-induced acidification closely followed the kinetics of  $\text{Cl}^-$  efflux, as the time course of the initial cell shrinkage and acidification were similar, and the maximum  $\text{Cl}^-$  and  $\text{OH}^-$  eq efflux rates coincided temporally. These results suggest that the  $\text{HCO}_3^-$  conductance pathway might be the same as that for  $\text{Cl}^-$ . We found that neither  $\text{Cl}^-$  nor  $\text{HCO}_3^-$  efflux in response to CCh was dependent on CFTR, as they were unaffected in cells isolated from *cftr*<sup>tm1Unc-/-</sup> mice (this study and Lee et al., 2007). This result was not surprising considering that CCh-evoked secretion rates measured from murine *cftr*<sup>tm1Unc-/-</sup> submucosal glands are identical to rates observed in Wt glands (Ianowski et al., 2007). To test the involvement of other  $\text{Cl}^-$  channels, we examined the effects of the nonspecific  $\text{Cl}^-$  channel inhibitor NFA, previously shown to inhibit CCh-evoked fluid secretion from intact murine submucosal glands (Ianowski et al., 2007). We found that NFA inhibited CCh-induced  $\text{Cl}^-$  efflux from isolated serous cells, strongly suggesting that non-CFTR  $\text{Cl}^-$  channels account for cholinergic-induced  $\text{Cl}^-$  secretion in murine serous acinar cells. Importantly, NFA also nearly completely blocked the cholinergic-induced acidification. The temporal coincidence of the  $\text{Cl}^-$  efflux and  $\text{HCO}_3^-$ -dependent acidification and their similar pharmacological sensitivities together suggest that  $\text{HCO}_3^-$  efflux is mediated by the same pathway that mediates  $\text{Ca}^{2+}$ -activated  $\text{Cl}^-$  efflux.

An important caveat to use of isolated cells is lack of information regarding the apical vs. basolateral polarization of the ion transport mechanisms examined, in particular the  $\text{Cl}^-$  and  $\text{HCO}_3^-$  efflux pathways experi-

mentally examined here. It is possible that a component of the  $\text{Cl}^-$  and  $\text{HCO}_3^-$  efflux we observed is mediated by basolaterally localized  $\text{Cl}^-$  channels. However, the accepted model of exocrine gland  $\text{Cl}^-$ /fluid secretion (for review see Melvin et al., 2005), supported by data from intact tissue preparations, is that the majority of secretagogue-regulated anion conductances are localized to the apical membrane, as basolaterally localized anion channels would “short circuit” the vectorial anion transport that drives fluid secretion. Cultured primary tracheal ciliated epithelial cells possess basolateral  $\text{Cl}^-$  channels (Fischer et al., 2007), but these likely play a role in fluid absorptive properties of the surface epithelium. Basolateral  $\text{Cl}^-$  channel expression has not been directly demonstrated for serous or other submucosal gland cell types. The simplest and most likely interpretation of our results is that the majority of secretagogue-stimulated  $\text{Cl}^-$  efflux we observed reflects CCh-evoked  $\text{Cl}^-$  secretion through the secretory  $\text{Cl}^-$  channel(s), as concluded in studies in other dispersed secretory acinar cells (for review see Melvin et al., 2005). This interpretation is further strongly supported by the similar NFA sensitivity of both CCh-induced acinar cell  $\text{Cl}^-$  efflux and intact gland fluid secretion.

Assuming that almost all of the CCh-stimulated  $\text{OH}^-$  eq efflux represents  $\text{HCO}_3^-$  efflux (as the ion substitution data suggest), and that the efflux pathway for  $\text{Cl}^-$  and  $\text{HCO}_3^-$  is the same (as the NFA data suggest), then the values determined for  $\text{HCO}_3^-$  and  $\text{Cl}^-$  fluxes can be used to provide a rough estimate of the  $\text{Cl}^-:\text{HCO}_3^-$  conductance ratio of the anion efflux pathway. The flux ( $J$ ) is equal to the product of the conductance ( $G$ ) and the driving force ( $DF$ ), or  $J = G \cdot DF$ , and  $J_{\text{Cl}^-}/J_{\text{HCO}_3^-} = (G_{\text{Cl}^-} \cdot DF_{\text{Cl}^-}) / (G_{\text{HCO}_3^-} \cdot DF_{\text{HCO}_3^-})$ .

The driving force is equal to the sum of the electrical and chemical driving force. While the membrane potential in these experiments is unknown, the electrical driving force for  $\text{HCO}_3^-$  and  $\text{Cl}^-$  efflux is the same since both are monovalent anions, allowing the electrical term to be ignored and requiring only a comparison of the concentration ratios. Thus,  $J_{\text{Cl}^-}/J_{\text{HCO}_3^-} = (G_{\text{Cl}^-} \cdot ([\text{Cl}^-]_i/[\text{Cl}^-]_o)) / (G_{\text{HCO}_3^-} \cdot ([\text{HCO}_3^-]_i/[\text{HCO}_3^-]_o))$ . At resting  $\text{pH}_i = 7.2$  and  $\text{pH}_o = 7.4$ ,  $[\text{HCO}_3^-]_i/[\text{HCO}_3^-]_o = 16 \text{ mM}/25 \text{ mM} = 0.64$ . Assuming resting  $[\text{Cl}^-]_i = 65 \text{ mM}$ ,  $[\text{Cl}^-]_i/[\text{Cl}^-]_o = 65 \text{ mM}/135 \text{ mM} = 0.48$ . Using the efflux rates determined during stimulation with CCh in the presence of  $30 \mu\text{M}$  DMA,  $-1.7 \text{ meq}\cdot\text{liter}^{-1}\cdot\text{s}^{-1}$  and  $-0.36 \text{ meq}\cdot\text{liter}^{-1}\cdot\text{s}^{-1}$  for  $\text{Cl}^-$  and  $\text{HCO}_3^-$ , respectively,  $G_{\text{Cl}^-}/G_{\text{HCO}_3^-} = (-1.7 \cdot 0.64)/(-0.36 \cdot 0.48) = 1.1/0.17 = 6.5$ .

This estimation gives a  $\text{Cl}^-/\text{HCO}_3^-$  conductance of  $\sim 6.5$ , similar to  $\text{Cl}^-/\text{HCO}_3^-$  conductance values ( $\sim 5$ ) previously reported for  $\text{Ca}^{2+}$ -activated  $\text{Cl}^-$  channels (Qu and Hartzell, 2000; for review see Hartzell et al., 2005). The ratio of fluxes and their mutual NFA sensitivity suggest that a  $\text{Ca}^{2+}$ -activated  $\text{Cl}^-$  channel serves a dual role in serous acinar cells as the primary cholinergic-activated

secretion pathway for both  $\text{Cl}^-$  and  $\text{HCO}_3^-$ . The identity of this  $\text{Ca}^{2+}$ -activated  $\text{Cl}^-$  channel(s) in the airway is/are yet to be determined, as is the expression of potential candidate channel proteins (bestrophins, etc.) in submucosal gland serous cells.

Taken together, our data suggest that CCh induces  $\text{HCO}_3^-$  secretion from airway gland serous cells. Previous work has demonstrated that cholinergic-induced fluid secretion by intact murine and porcine glands is significantly blocked by removal of  $\text{CO}_2$ – $\text{HCO}_3^-$  from the extracellular medium (Inglis et al., 1997a, 1998; Ballard et al., 1999; Joo et al., 2001a,b, 2002b; Ianowski et al., 2007). While these data suggest that  $\text{HCO}_3^-$  plays an important role in secretion, they are difficult to interpret, since inhibition could be caused by either a primary defect of serous cell secretion or defective modification of secreted fluid elsewhere in the gland. Our results suggest that CCh-evoked murine serous cell fluid secretion does not depend strongly on the presence of  $\text{HCO}_3^-$ , as we observed little effect of removal of  $\text{HCO}_3^-$  on CCh-evoked  $\text{Cl}^-$  dynamics, and our previous data showed that basolateral  $\text{Cl}^-$  accumulation is primarily dependent on NKCC1 and not NHE/AE.

We previously concluded that serous cell volume changes in response to CCh are due almost entirely due to a loss of KCl content (Lee et al., 2007). Our results here indicate that a portion also reflects loss of  $\text{KHCO}_3$ . However, the  $\text{HCO}_3^-$  content lost is small, as  $[\text{HCO}_3^-]_i$  would be expected to fall at most from  $\sim 16$  mM (at  $\text{pH}_i = 7.2$ ) to  $\sim 12$  mM at ( $\text{pH}_i = 7.0$ ; the approximate  $\text{pH}_i$  after stimulation with  $100 \mu\text{M}$  CCh +  $30 \mu\text{M}$  DMA). Taking into account the change in cell volume ( $V/V_0$  from 1 to  $\sim 0.8$ ), the cells would have lost at most  $(16 \text{ meq} \cdot \text{liter}^{-1} \times 1) - (12 \text{ meq} \cdot \text{liter}^{-1} \times 0.8) = \sim 6.4 \text{ meq} \cdot \text{liter}^{-1}$  of  $\text{HCO}_3^-$  content. This is approximately sevenfold less than the  $44 \text{ meq} \cdot \text{liter}^{-1}$  of  $\text{Cl}^-$  content lost during CCh stimulation (Lee et al., 2007). In reality, the cells lose even less, because activation of NHE1 restores lost  $\text{HCO}_3^-$  content by raising  $\text{pH}_i$  and enabling  $\text{CO}_2$  to be continuously hydrated to form  $\text{HCO}_3^-$ .

Optical measurements of conductive  $\text{Cl}^-$  and  $\text{HCO}_3^-$  effluxes are not as direct as electrophysiological characterization of  $\text{HCO}_3^-$  and  $\text{Cl}^-$  currents. However, we have found patch clamp electrophysiology of murine serous acinar cells to be challenging because seal formation is rare, likely due to the presence of connective tissue that has been difficult to remove without overdigesting and killing the cells. Alternately, our optical approaches have enabled study of these pathways in intact cells with intact signal transduction mechanisms, and they have enabled us to elucidate the contributions (or lack thereof) of electroneutral processes such as  $\text{Na}^+/\text{H}^+$  or  $\text{Cl}^-/\text{HCO}_3^-$  exchange.

#### NHE1 Sustains $\text{HCO}_3^-$ Secretion

Our data suggest that NHE1 activity in airway serous acinar cells is strongly up-regulated in response to CCh

stimulation. Aside from the ubiquitous role of NHE1 in  $\text{pH}_i$  homeostasis in almost all cell types, NHE1 has been coopted by secretory epithelia to serve a variety of functions. Basolaterally expressed NHE1 functions in combination with  $\text{Cl}^-/\text{HCO}_3^-$  exchangers to facilitate  $\text{Cl}^-$  accumulation and sustain transepithelial  $\text{Cl}^-$  secretion in the parotid gland (Robertson and Foskett, 1994; for review see Melvin et al., 2005). However, in the murine airway submucosal gland serous cells studied here, the primary function of NHE1 appears to be to raise  $\text{pH}_i$  during stimulated fluid secretion. By keeping  $\text{pH}_i$  elevated during agonist-activated  $\text{HCO}_3^-$  efflux, basolateral NHE1 can act as a major mechanism to sustain  $\text{HCO}_3^-$  secretion.

Ballard and colleagues demonstrated that DMA inhibited  $>50\%$  of bumetanide-insensitive liquid secretion and nearly  $50\%$  of  $\text{HCO}_3^-$  secretion by excised porcine bronchi (Trout et al., 1998a, 2001) and that DMA affected the composition of fluid and mucus secreted from intact porcine submucosal glands (Inglis et al., 1997a, 1998; Trout et al., 1998b). Our results here suggest that those observations could be accounted for, at least in part, by DMA inhibition of NHE1-dependent sustained  $\text{HCO}_3^-$  secretion from submucosal gland serous acini. In the future, the methods described here will be translated to isolated porcine serous cells to test this hypothesis.

The molecular mechanisms of cholinergic activation of NHE1 in murine airway serous acinar cells is unclear. It is unlikely that the initial  $\text{HCO}_3^-$  efflux is a signal, since agonist-induced alkalization was observed in the absence of a strong initial acidification when the cells were stimulated in  $\text{CO}_2$ – $\text{HCO}_3^-$ -free conditions. Muscarinic activation of NHE1 in salivary acinar cells is mediated by increased  $[\text{Ca}^{2+}]_i$ , independent of calmodulin and PKC (Manganel and Turner, 1989, 1990, 1991; Okada et al., 1991; Robertson et al., 1997), whereas recombinant NHE1 requires calmodulin and/or PKC for agonist-induced activation (for reviews see Putney et al., 2002; Malo and Fliegel, 2006). Whether these pathways are required for NHE1 activation in airway serous acinar cells remains to be determined.

Our data support the existence of other  $\text{Na}^+$ -dependent, but DMA-insensitive, mechanisms in serous cells that play an important role in regulating resting  $\text{pH}_i$ , in agreement with conclusions reached in intact porcine submucosal glands (Hug and Bridges, 2001). The identity and role of other  $\text{H}^+$  and/or  $\text{HCO}_3^-$ -linked transporters, including NBC isoforms, remains to be elucidated.

#### Possible Importance of Serous Cell $\text{HCO}_3^-$ Secretion for Normal and Pathogenic Airway Fluid Homeostasis

The secreted fluid product from intact submucosal glands has been consistently determined to be near or slightly less than neutral pH (Jayaraman et al., 2001; Joo et al., 2001a; Song et al., 2006). However, our results suggest that serous acinar cells secrete a primary alkaline fluid.



Unless serous cells possess unknown mechanisms to further modify rates or amounts of  $\text{HCO}_3^-$  secretion that have remained undetected in our experiments, these results suggest that fluid secreted by serous cells may be modified by other cell types during its transit to the airway surface epithelium. It is possible that an initial alkaline pH of the primary secreted fluid is important as it washes past mucous cells and hydrates released mucous granules. Modifications of the primary secreted fluid may be accomplished by ion transport mechanisms in mucous and/or collecting duct cells that are still unknown. The methods presented here could be adapted to study ion transport pathways in these cell types.

In the genetic disease CF, it has been speculated that lung disease may be due not only to a reduced quantity, but also to altered composition of the ASL. In particular, it has been speculated that  $\text{HCO}_3^-$  secretion and regulation of ASL pH may play an important role in CF pathology (for review see Quinton, 1999, 2001). It has been suggested that CF ASL may be acidic compared with normal ASL (for review see Coakley and Boucher, 2001), and that isolated intact submucosal glands from CF patients produce a hyperacidic product compared with control glands (Song et al., 2006), although the mechanisms involved are unknown. Our data suggest that serous acinar cells can support  $\text{HCO}_3^-$  secretion in response to cholinergic stimulation, likely through a  $\text{Ca}^{2+}$ -activated  $\text{Cl}^-$  channel. Because cholinergic-stimulated secretion in CF submucosal glands is intact, this supports the possibility that the  $\text{Ca}^{2+}$ -stimulated secretion pathway and/or alternative  $\text{Cl}^-$  channels may be important therapeutic targets for CF treatment if impairment of cAMP-activated  $\text{HCO}_3^-$  secretion from serous cells contributes to CF pathology. However, it still remains to be determined if serous acinar cells secrete  $\text{HCO}_3^-$  in response to cAMP agonists, and whether any cAMP-induced  $\text{HCO}_3^-$  secretion is altered in cells lacking functional CFTR. In the future, the optical techniques developed and outlined in this study will be used to examine the role of cAMP and CFTR in serous cell  $\text{HCO}_3^-$  secretion to begin to address whether this process is impaired in CF.

The authors wish to thank Dr. D.-O.D. Mak for assistance with analyses of flux data, Dr. R.J. Turner for antibody to NKCC1, Dr. J. Puentner (Sanofi-Aventis, Frankfurt, Germany) for gifts of cariporide and S3226, and Ms. R. Munden for excellent animal assistance.

R.J. Lee was supported by predoctoral fellowships from the National Science Foundation and the Cystic Fibrosis Foundation. J.M. Harlow was supported by RDP-R881 from the Cystic Fibrosis Foundation. This study was funded by grant FOSKET07G0 from the Cystic Fibrosis Foundation to J.K. Foskett.

Angus C. Nairn served as editor.

Submitted: 4 April 2008

Accepted: 27 May 2008

## REFERENCES

- Baird, N.R., J. Orlowski, E.Z. Szabo, H.C. Zaun, P.J. Schultheis, A.G. Menon, and G.E. Shull. 1999. Molecular cloning, genomic organization, and functional expression of  $\text{Na}^+/\text{H}^+$  exchanger isoform 5 (NHE5) from human brain. *J. Biol. Chem.* 274:4377–4382.
- Ballard, S.T., and S.K. Inglis. 2004. Liquid secretion properties of airway submucosal glands. *J. Physiol.* 556:1–10.
- Ballard, S.T., and D. Spadafora. 2007. Fluid secretion by submucosal glands of the tracheobronchial airways. *Respir. Physiol. Neurobiol.* 159:271–277.
- Ballard, S.T., L. Trout, Z. Bebok, E.J. Sorscher, and A. Crews. 1999. CFTR involvement in chloride, bicarbonate, and liquid secretion by airway submucosal glands. *Am. J. Physiol.* 277:L694–L699.
- Becker, A.M., J. Zhang, S. Goyal, V. Dwarakanath, P.S. Aronson, O.W. Moe, and M. Baum. 2007. Ontogeny of NHE8 in the rat proximal tubule. *Am. J. Physiol. Renal Physiol.* 293:F255–F261.
- Boron, W.F. 2004. Regulation of intracellular pH. *Adv. Physiol. Educ.* 28:160–179.
- Boron, W.F., and P. De Weer. 1976. Intracellular pH transients in squid giant axons caused by  $\text{CO}_2$ ,  $\text{NH}_3$ , and metabolic inhibitors. *J. Gen. Physiol.* 67:91–112.
- Brown, D.A., J.E. Melvin, and D.I. Yule. 2003. Critical role for NHE1 in intracellular pH regulation in pancreatic acinar cells. *Am. J. Physiol. Gastrointest. Liver Physiol.* 285:G804–G812.
- Buckler, K.J., and R.D. Vaughan-Jones. 1990. Application of a new pH-sensitive fluoroprobe (carboxy-SNARF-1) for intracellular pH measurement in small, isolated cells. *Pflügers Arch.* 417:234–239.
- Chambrey, R., J.M. Achard, and D.G. Warnock. 1997. Heterologous expression of rat NHE4: a highly amiloride-resistant  $\text{Na}^+/\text{H}^+$  exchanger isoform. *Am. J. Physiol.* 272:C90–C98.
- Chambrey, R., P.L. St John, D. Eladari, F. Quentin, D.G. Warnock, D.R. Abrahamson, R.A. Pódevin, and M. Paillard. 2001. Localization and functional characterization of  $\text{Na}^+/\text{H}^+$  exchanger isoform NHE4 in rat thick ascending limbs. *Am. J. Physiol. Renal Physiol.* 281:F707–F717.
- Coakley, R.D., and R.C. Boucher. 2001. Regulation and functional significance of airway surface liquid pH. *JOP.* 2:294–300.
- Eberwine, J. 2001. Single-cell molecular biology. *Nat. Neurosci.* 4(Suppl):1155–1156.
- Engelhardt, J.F., J.R. Yankaskas, S.A. Ernst, Y. Yang, C.R. Marino, R.C. Boucher, J.A. Cohn, and J.M. Wilson. 1992. Submucosal glands are the predominant site of CFTR expression in the human bronchus. *Nat. Genet.* 2:240–248.
- Evans, R.L., S.M. Bell, P.J. Schultheis, G.E. Shull, and J.E. Melvin. 1999. Targeted disruption of the Nhe1 gene prevents muscarinic agonist-induced up-regulation of  $\text{Na}^+/\text{H}^+$  exchange in mouse parotid acinar cells. *J. Biol. Chem.* 274:29025–29030.
- Fischer, H., B. Illek, W.E. Finkbeiner, and J.H. Widdicombe. 2007. Basolateral  $\text{Cl}^-$  channels in primary airway epithelial cultures. *Am. J. Physiol. Lung Cell. Mol. Physiol.* 292:L1432–L1443.
- Foskett, J.K. 1988. Simultaneous Nomarski and fluorescence imaging during video microscopy of cells. *Am. J. Physiol.* 255:C566–C571.
- Foskett, J.K. 1990a.  $[\text{Ca}^{2+}]_i$  modulation of  $\text{Cl}^-$  content controls cell volume in single salivary acinar cells during fluid secretion. *Am. J. Physiol.* 259:C998–C1004.
- Foskett, J.K. 1990b. Optical studies of ion and water transport in single living cells. In *Noninvasive Techniques in Cell Biology*. J.K. Foskett and S. Grinstein, editors. Wiley-Liss, Inc., New York. 237–272.
- Foskett, J.K. 1993. Optical imaging of ion transport in single living cells. *Comments Mol. Cell. Biophys.* 8:115–135.
- Gerelsaikh, T., and R.J. Turner. 2000. Membrane topology and function of the secretory  $\text{Na}^+-\text{K}^+-2\text{Cl}^-$  cotransporter (NKCC1). *J. Korean Med. Sci.* 15(Suppl):S3–S4.

- Goyal, S., G. Vanden Heuvel, and P.S. Aronson. 2003. Renal expression of novel  $\text{Na}^+/\text{H}^+$  exchanger isoform NHE8. *Am. J. Physiol. Renal Physiol.* 284:F467–F473.
- Goyal, S., S. Mentone, and P.S. Aronson. 2005. Immunolocalization of NHE8 in rat kidney. *Am. J. Physiol. Renal Physiol.* 288:F530–F538.
- Grubb, B.R., and R.C. Boucher. 1999. Pathophysiology of gene-targeted mouse models for cystic fibrosis. *Physiol. Rev.* 79:S193–S214.
- Haas, M., and B. Forbush III. 2000. The Na-K-Cl cotransporter of secretory epithelia. *Annu. Rev. Physiol.* 62:515–534.
- Hartzell, C., I. Putzier, and J. Arreola. 2005. Calcium-activated chloride channels. *Annu. Rev. Physiol.* 67:719–758.
- Huang, P., E. Gilmore, P. Kultgen, P. Barnes, S. Milgram, and M.J. Stutts. 2004. Local regulation of cystic fibrosis transmembrane regulator and epithelial sodium channel in airway epithelium. *Proc. Am. Thorac. Soc.* 1:33–37.
- Hug, M.J., and R.J. Bridges. 2001. pH regulation and bicarbonate transport of isolated porcine submucosal glands. *JOP.* 2:274–279.
- Ianowski, J.P., J.Y. Choi, J.J. Wine, and J.W. Hanrahan. 2007. Mucus secretion by single tracheal submucosal glands from normal and CFTR knock-out mice. *J. Physiol.* 580:301–314.
- Inglis, S.K., M.R. Corboz, A.E. Taylor, and S.T. Ballard. 1997a. Effect of anion transport inhibition on mucus secretion by airway submucosal glands. *Am. J. Physiol.* 272:L372–L377.
- Inglis, S.K., M.R. Corboz, A.E. Taylor, and S.T. Ballard. 1997b. In situ visualization of bronchial submucosal glands and their secretory response to acetylcholine. *Am. J. Physiol.* 272:L203–L210.
- Inglis, S.K., M.R. Corboz, and S.T. Ballard. 1998. Effect of anion secretion inhibitors on mucin content of airway submucosal gland ducts. *Am. J. Physiol.* 274:L762–L766.
- Jacquot, J., E. Puchelle, J. Hinnrasky, C. Fuchey, C. Bettinger, C. Spilmont, N. Bonnet, A. Dieterle, D. Dreyer, A. Pavirani, et al. 1993. Localization of the cystic fibrosis transmembrane conductance regulator in airway secretory glands. *Eur. Respir. J.* 6:169–176.
- Jayaraman, S., N.S. Joo, B. Reitz, J.J. Wine, and A.S. Verkman. 2001. Submucosal gland secretions in airways from cystic fibrosis patients have normal  $[\text{Na}^+]$  and pH but elevated viscosity. *Proc. Natl. Acad. Sci. USA.* 98:8119–8123.
- Joo, N.S., M.E. Krouse, J.V. Wu, Y. Saenz, S. Jayaraman, A.S. Verkman, and J.J. Wine. 2001a.  $\text{HCO}_3^-$  transport in relation to mucus secretion from submucosal glands. *JOP.* 2:280–284.
- Joo, N.S., J.V. Wu, M.E. Krouse, Y. Saenz, and J.J. Wine. 2001b. Optical method for quantifying rates of mucus secretion from single submucosal glands. *Am. J. Physiol. Lung Cell. Mol. Physiol.* 281:L458–L468.
- Joo, N.S., T. Irokawa, J.V. Wu, R.C. Robbins, R.I. Whyte, and J.J. Wine. 2002a. Absent secretion to vasoactive intestinal peptide in cystic fibrosis airway glands. *J. Biol. Chem.* 277:50710–50715.
- Joo, N.S., Y. Saenz, M.E. Krouse, and J.J. Wine. 2002b. Mucus secretion from single submucosal glands of pig. Stimulation by carbachol and vasoactive intestinal peptide. *J. Biol. Chem.* 277:28167–28175.
- Joo, N.S., T. Irokawa, R.C. Robbins, and J.J. Wine. 2006. Hyposecretion, not hyperabsorption, is the basic defect of cystic fibrosis airway glands. *J. Biol. Chem.* 281:7392–7398.
- Kang'ethe, W., K.G. Aimanova, A.K. Pullikuth, and S.S. Gill. 2007. NHE8 mediates amiloride-sensitive  $\text{Na}^+/\text{H}^+$  exchange across mosquito Malpighian tubules and catalyzes  $\text{Na}^+$  and  $\text{K}^+$  transport in reconstituted proteoliposomes. *Am. J. Physiol. Renal Physiol.* 292:F1501–F1512.
- Klanke, C.A., Y.R. Su, D.F. Callen, Z. Wang, P. Meneton, N. Baird, R.A. Kandasamy, J. Orlowski, B.E. Otterud, M. Leppert, et al. 1995. Molecular cloning and physical and genetic mapping of a novel human  $\text{Na}^+/\text{H}^+$  exchanger (NHE5/SLC9A5) to chromosome 16q22.1. *Genomics.* 25:615–622.
- Ko, S.B., W. Zeng, M.R. Dorwart, X. Luo, K.H. Kim, L. Millen, H. Goto, S. Naruse, A. Soyombo, P.J. Thomas, and S. Muallem. 2004. Gating of CFTR by the STAS domain of SLC26 transporters. *Nat. Cell Biol.* 6:343–350.
- Lee, M.G., J.Y. Choi, X. Luo, E. Strickland, P.J. Thomas, and S. Muallem. 1999a. Cystic fibrosis transmembrane conductance regulator regulates luminal  $\text{Cl}^-/\text{HCO}_3^-$  exchange in mouse submandibular and pancreatic ducts. *J. Biol. Chem.* 274:14670–14677.
- Lee, M.G., W.C. Wigley, W. Zeng, L.E. Noel, C.R. Marino, P.J. Thomas, and S. Muallem. 1999b. Regulation of  $\text{Cl}^-/\text{HCO}_3^-$  exchange by cystic fibrosis transmembrane conductance regulator expressed in NIH 3T3 and HEK 293 cells. *J. Biol. Chem.* 274:3414–3421.
- Lee, R.J., M.P. Limberis, M.F. Hennessey, J.M. Wilson, and J.K. Foskett. 2007. Optical imaging of  $\text{Ca}^{2+}$ -evoked fluid secretion by murine nasal submucosal gland serous acinar cells. *J. Physiol.* 582:1099–1124.
- Lee, S.H., T. Kim, E.S. Park, S. Yang, D. Jeong, Y. Choi, and J. Rho. 2008. NHE10, a novel osteoclast-specific member of the  $\text{Na}^+/\text{H}^+$  exchanger family, regulates osteoclast differentiation and survival. *Biochem. Biophys. Res. Commun.* 369:320–326.
- Liu, J., Z. Diwu, and W.Y. Leung. 2001. Synthesis and photophysical properties of new fluorinated benzo[c]xanthene dyes as intracellular pH indicators. *Bioorg. Med. Chem. Lett.* 11:2903–2905.
- Malo, M.E., and L. Fliegel. 2006. Physiological role and regulation of the  $\text{Na}^+/\text{H}^+$  exchanger. *Can. J. Physiol. Pharmacol.* 84:1081–1095.
- Manganel, M., and R.J. Turner. 1989. Agonist-induced activation of  $\text{Na}^+/\text{H}^+$  exchange in rat parotid acinar cells. *J. Membr. Biol.* 111:191–198.
- Manganel, M., and R.J. Turner. 1990. Agonist-induced activation of  $\text{Na}^+/\text{H}^+$  exchange in rat parotid acinar cells is dependent on calcium but not on protein kinase C. *J. Biol. Chem.* 265:4284–4289.
- Manganel, M., and R.J. Turner. 1991. Rapid secretagogue-induced activation of  $\text{Na}^+/\text{H}^+$  exchange in rat parotid acinar cells. Possible interrelationship between volume regulation and stimulus-secretion coupling. *J. Biol. Chem.* 266:10182–10188.
- Masereel, B., L. Pochet, and D. Laeckmann. 2003. An overview of inhibitors of  $\text{Na}^+/\text{H}^+$  exchanger. *Eur. J. Med. Chem.* 38:547–554.
- Melvin, J.E., D. Yule, T. Shuttleworth, and T. Begenisich. 2005. Regulation of fluid and electrolyte secretion in salivary gland acinar cells. *Annu. Rev. Physiol.* 67:445–469.
- Nakamura, N., S. Tanaka, Y. Teko, K. Mitsui, and H. Kanazawa. 2005. Four  $\text{Na}^+/\text{H}^+$  exchanger isoforms are distributed to Golgi and post-Golgi compartments and are involved in organelle pH regulation. *J. Biol. Chem.* 280:1561–1572.
- Nguyen, H.V., G.E. Shull, and J.E. Melvin. 2000. Muscarinic receptor-induced acidification in sublingual mucous acinar cells: loss of pH recovery in  $\text{Na}^+/\text{H}^+$  exchanger-1 deficient mice. *J. Physiol.* 523(Pt 1):139–146.
- Nguyen, H.V., A. Stuart-Tilley, S.L. Alper, and J.E. Melvin. 2004.  $\text{Cl}^-/\text{HCO}_3^-$  exchange is acetazolamide sensitive and activated by a muscarinic receptor-induced  $[\text{Ca}^{2+}]_i$  increase in salivary acinar cells. *Am. J. Physiol. Gastrointest. Liver Physiol.* 286:G312–G320.
- Okada, M., Y. Saito, E. Sawada, and A. Nishiyama. 1991. Microfluorimetric imaging study of the mechanism of activation of the  $\text{Na}^+/\text{H}^+$  antiport by muscarinic agonist in rat mandibular acinar cells. *Pflugers Arch.* 419:338–348.
- Orlowski, J., and S. Grinstein. 2004. Diversity of the mammalian sodium/proton exchanger SLC9 gene family. *Pflugers Arch.* 447:549–565.
- Park, K., J.A. Olchowka, L.A. Richardson, C. Bookstein, E.B. Chang, and J.E. Melvin. 1999. Expression of multiple  $\text{Na}^+/\text{H}^+$  exchanger isoforms in rat parotid acinar and ductal cells. *Am. J. Physiol.* 276:G470–G478.
- Park, K., R.L. Evans, G.E. Watson, K. Nehrke, L. Richardson, S.M. Bell, P.J. Schultheis, A.R. Hand, G.E. Shull, and J.E. Melvin. 2001. Defective fluid secretion and NaCl absorption in the parotid glands of  $\text{Na}^+/\text{H}^+$  exchanger-deficient mice. *J. Biol. Chem.* 276:27042–27050.

- Park, M., S.B. Ko, J.Y. Choi, G. Muallem, P.J. Thomas, A. Pushkin, M.S. Lee, J.Y. Kim, M.G. Lee, S. Muallem, and I. Kurtz. 2002. The cystic fibrosis transmembrane conductance regulator interacts with and regulates the activity of the  $\text{HCO}_3^-$  salvage transporter human  $\text{Na}^+\text{-HCO}_3^-$  cotransport isoform 3. *J. Biol. Chem.* 277:50503–50509.
- Parvin, M.N., T. Gerelsaikhan, and R.J. Turner. 2007. Regions in the cytosolic C-terminus of the secretory  $\text{Na}^+\text{-K}^+\text{-2Cl}^-$  cotransporter NKCC1 are required for its homodimerization. *Biochemistry.* 46:9630–9637.
- Poulsen, J.H., H. Fischer, B. Illek, and T.E. Machen. 1994. Bicarbonate conductance and pH regulatory capability of cystic fibrosis transmembrane conductance regulator. *Proc. Natl. Acad. Sci. USA.* 91:5340–5344.
- Putney, L.K., S.P. Denker, and D.L. Barber. 2002. The changing face of the  $\text{Na}^+/\text{H}^+$  exchanger, NHE1: structure, regulation, and cellular actions. *Annu. Rev. Pharmacol. Toxicol.* 42:527–552.
- Qu, Z.H., and C. Hartzell. 2000. Anion permeation in  $\text{Ca}^{2+}$ -activated  $\text{Cl}^-$  channels. *J. Gen. Physiol.* 116:825–844.
- Quinton, P.M. 1999. Physiological basis of cystic fibrosis: a historical perspective. *Physiol. Rev.* 79:S3–S22.
- Quinton, P.M. 2001. The neglected ion:  $\text{HCO}_3^-$ . *Nat. Med.* 7:292–293.
- Raphael, G.D., E.V. Jeney, J.N. Baraniuk, I. Kim, S.D. Meredith, and M.A. Kaliner. 1989. Pathophysiology of rhinitis. Lactoferrin and lysozyme in nasal secretions. *J. Clin. Invest.* 84:1528–1535.
- Renner, E.L., J.R. Lake, M. Persico, and B.F. Scharschmidt. 1989.  $\text{Na}^+\text{-H}^+$  exchange activity in rat hepatocytes: role in regulation of intracellular pH. *Am. J. Physiol.* 256:G44–G52.
- Robertson, M.A., and J.K. Foskett. 1994.  $\text{Na}^+$  transport pathways in secretory acinar cells: membrane cross talk mediated by  $[\text{Cl}^-]_i$ . *Am. J. Physiol.* 267:C146–C156.
- Robertson, M.A., M. Woodside, J.K. Foskett, J. Orlowski, and S. Grinstein. 1997. Muscarinic agonists induce phosphorylation-independent activation of the NHE-1 isoform of the  $\text{Na}^+/\text{H}^+$  antiporter in salivary acinar cells. *J. Biol. Chem.* 272:287–294.
- Roos, A., and W.F. Boron. 1981. Intracellular pH. *Physiol. Rev.* 61:296–434.
- Salinas, D., P.M. Haggie, J.R. Thiagarajah, Y. Song, K. Rosbe, W.E. Finkbeiner, D.W. Nielson, and A.S. Verkman. 2005. Submucosal gland dysfunction as a primary defect in cystic fibrosis. *FASEB J.* 19:431–433.
- Schwark, J.R., H.W. Jansen, H.J. Lang, W. Krick, G. Burckhardt, and M. Hropot. 1998. S3226, a novel inhibitor of  $\text{Na}^+/\text{H}^+$  exchanger subtype 3 in various cell types. *Pflugers Arch.* 436:797–800.
- Song, Y., and A.S. Verkman. 2001. Aquaporin-5 dependent fluid secretion in airway submucosal glands. *J. Biol. Chem.* 276:41288–41292.
- Song, Y., D. Salinas, D.W. Nielson, and A.S. Verkman. 2006. Hyperacidity of secreted fluid from submucosal glands in early cystic fibrosis. *Am. J. Physiol. Cell Physiol.* 290:C741–C749.
- Thiagarajah, J.R., Y. Song, P.M. Haggie, and A.S. Verkman. 2004. A small molecule CFTR inhibitor produces cystic fibrosis-like submucosal gland fluid secretions in normal airways. *FASEB J.* 18:875–877.
- Thomas, R.C. 1984. Experimental displacement of intracellular pH and the mechanism of its subsequent recovery. *J. Physiol.* 354:3P–22P.
- Trout, L., J.T. Gatzky, and S.T. Ballard. 1998a. Acetylcholine-induced liquid secretion by bronchial epithelium: role of  $\text{Cl}^-$  and  $\text{HCO}_3^-$  transport. *Am. J. Physiol.* 275:L1095–L1099.
- Trout, L., M. King, W. Feng, S.K. Inglis, and S.T. Ballard. 1998b. Inhibition of airway liquid secretion and its effect on the physical properties of airway mucus. *Am. J. Physiol.* 274:L258–L263.
- Trout, L., M.R. Corboz, and S.T. Ballard. 2001. Mechanism of substance P-induced liquid secretion across bronchial epithelium. *Am. J. Physiol. Lung Cell. Mol. Physiol.* 281:L639–L645.
- Van Gelder, R.N., M.E. von Zastrow, A. Yool, W.C. Dement, J.D. Barchas, and J.H. Eberwine. 1990. Amplified RNA synthesized from limited quantities of heterogeneous cDNA. *Proc. Natl. Acad. Sci. USA.* 87:1663–1667.
- Wang, D., S.M. King, T.A. Quill, L.K. Doolittle, and D.L. Garbers. 2003. A new sperm-specific  $\text{Na}^+/\text{H}^+$  exchanger required for sperm motility and fertility. *Nat. Cell Biol.* 5:1117–1122.
- Weintraub, W.H., and T.E. Machen. 1989. pH regulation in hepatoma cells: roles for Na-H exchange,  $\text{Cl-HCO}_3$  exchange, and Na- $\text{HCO}_3$  cotransport. *Am. J. Physiol.* 257:G317–G327.
- Wine, J.J., and N.S. Joo. 2004. Submucosal glands and airway defense. *Proc. Am. Thorac. Soc.* 1:47–53.
- Wu, J.V., M. Krouse, and J.J. Wine. 2006. Acinar origin of Cftr-dependent airway submucosal gland fluid secretion. *Am. J. Physiol. Lung Cell Mol. Physiol.* 292:L304–L311.
- Yang, C.M., J.M. Farley, and T.M. Dwyer. 1988. Muscarinic stimulation of submucosal glands in swine trachea. *J. Appl. Physiol.* 64:200–209.
- Zachos, N.C., M. Tse, and M. Donowitz. 2005. Molecular physiology of intestinal  $\text{Na}^+/\text{H}^+$  exchange. *Annu. Rev. Physiol.* 67:411–443.
- Zhang, J., I.A. Bobulescu, S. Goyal, P.S. Aronson, M.G. Baum, and O.W. Moe. 2007. Characterization of  $\text{Na}^+/\text{H}^+$  exchanger NHE8 in cultured renal epithelial cells. *Am. J. Physiol. Renal Physiol.* 293:F761–F766.